ABSTRACT

Title of Thesis: EFFECT OF ENCAPSULANT ON HIGH-TEMPERATURE RELIABILITY OF THE GOLD WIREBOND – ALUMINUM BONDPAD INTERFACE

Arvind Chandrasekaran, Master of Science, 2003

Thesis Directed By: Dr. F. Patrick McCluskey
Department of Mechanical Engineering

Conventional plastic encapsulated microcircuits (PEMs) are increasingly being used in harsh environments such as automotive, well-logging, aerospace and military applications. There is a need, therefore, to examine their performance and reliability at high temperatures. A commonly used first level interconnect in PEMs is the gold wirebond – aluminum bondpad interface. This interface has been found to have a very limited life at temperatures above 180 °C, due to intermetallic formation and subsequent corrosion. The corrosion is caused by brominated flame retardants and antimony trioxide in the molding compound. Given a set of environmental requirements, it is necessary to choose the right PEM for that set and to predict the life of the PEM based on the effect the flame retardants will have on the wirebond-bondpad interface. It is also necessary to look for better molding compound alternatives, such as environmentally-friendly

halogen-free compounds, to mitigate high temperature corrosion. Thus, the focus of this study is to characterize the Br-related wirebond weakening process and to establish the high temperature reliability of halogen-free molding compounds. Several conventional PEMs have been tested at high temperature, and the wirebond strength profile has been found. A set of next-generation molding compound PEMs have also been tested at high temperature and high humidity, and their life at those conditions has been determined.

EFFECT OF ENCAPSULANT ON HIGH-TEMPERATURE RELIABILITY OF THE GOLD WIREBOND – ALUMINUM BONDPAD INTERFACE

By
Arvind Chandrasekaran

Thesis submitted to the Faculty of the Graduate School of the
University of Maryland, College Park in partial fulfillment
of requirements for the degree of
Master of Science
2003

Advisory Committee:

Associate Professor Patrick McCluskey
Associate Professor David Bigio
Associate Professor Peter Sandborn

TABLE OF CONTENTS

LIST OF TABLES

LIST OF FIGURES

1 Introduction

By eliminating cabling, distributed system architechtures reduce cost, size & weight, improve reliability, decrease suceptibility to electromagnetic interference (EMI), lower noise and signal attenuation, and provide easy maintenance. In this way, distributed system architechtures can improve performance in many different applications from avionics to well-logging. In a distributed system architecture, the sensors, processors and actuators are all housed in a single, remotely-placed unit. The factor limiting the widespread acceptance of distributed control systems, however, is the need to operate the electronics at the ambient temperature of the application, which typically exceeds the traditional maximum allowable operating temperatures. Examples of candidates for the utilization of high temperature electronics, air and ground vehicles, have both regions of high temperature, such as engines, and severe limitations on weight. The weight restrictions pose a limitation on the ability to use large amounts of cabling to transfer signals to and from a remotely cooled processing unit along with a limitation on the size and extent of the cooling units. The limitations on cooling have been the impetus, to a great extent, for the development of high temperature electronics. Although the devices producing the reject heat are, generally speaking, small and lightweight, and it is generally easy to remove the heat from the device generating it, disposing of that heat is a somewhat daunting enterprise. The only available medium for accepting the rejected heat is often ambient air. If natural or forced convection air cooling is not practical due to temperature differential, gas volume or ambient dust conditions, liquid cooling, either single or two phase, is necessary. Liquid to air heat exchangers are notoriously large,

making severe demands on allowable weight and volume from the vehicles. Such systems also require pumps or compressors, coolant piping, and controls, which make additional demands on weight and volume [1]. Furthermore, often the only cooling fluid is the engine fuel which can be at quite high reject temperatures. Development of electronic systems that can operate at local ambient temperatures up to 200°C without cooling is therefore seen as a critical technology for the 21st century.

Traditionally, commercial electronic devices have been designed to operate within a small temperature window, with a ceiling of 70°C, or 125°C in some military and avionic applications. Specialty devices in ceramic packages were used for applications requiring high temperature operation. These specialty devices in ceramic packaging are not the preferred choice nowadays as their cost is increasing and the supply is decreasing. Conventional plastic encapsulated microcircuits (PEMs) are increasingly being used in harsh environments such as automotive, oilfield services, aerospace and military applications. There is a need, therefore, to examine their performance and reliability at high temperatures.

According to a report released in 2000 by the High temperature Electronics Network (HITEN), the world market for high temperature electronics is expected to increase from $177 million in 1998 to $887 million by the year 2008, increasing the need for components reliable at high temperatures (Figure 1).

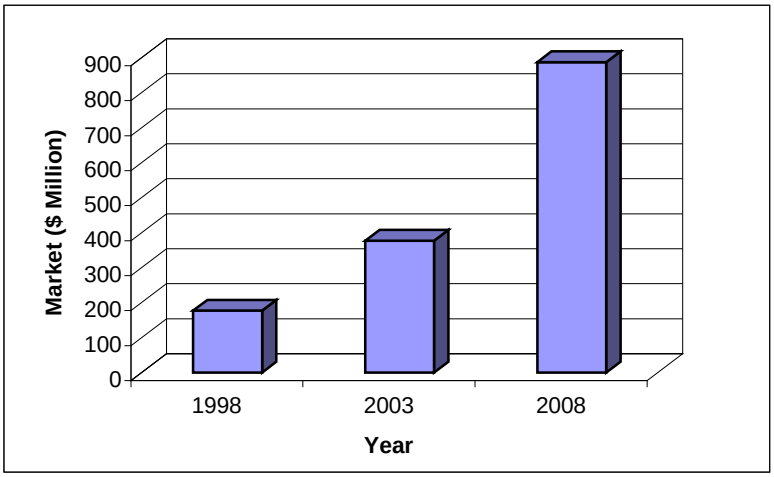

Figure 1: High Temperature Electronics Market

Some of the major application areas and associated temperatures of exposure are shown in Table 1.

Well Logging Instrumentation	
Oil and gas wells	75 °C to 225 °C
Steam injection	200 °C to 300 °C
Geothermal walls	200 °C to 350 °C
Aerospace	
Electronic braking system	Up to 250 °C
Engine control/monitoring	Up to 300 °C
Automotive	
Engine compartment	Up to 165 °C
On-engine and on-transmission	Up to 165 °C
Wheel mounted components	Up to 250 °C
Others	
Exploration vehicles	Up to 500 °C
Space systems	Up to 400 °C
Nuclear reactor monitoring	Up to 550 °C
Gas Turbine Engines	55 °C to 1200 °C

Table 1: High Temperature Applications [1]

It is seen that the applications for high temperature electronics are numerous. Many of the applications, such as on-engine automotive electronics for improved fuel efficiency require high temperature operation under 200°C when PEMs might be an option. Automotive applications are very cost-sensitive and would benefit from PEMs if they could beshown to be reliable over the wide temperature range.

In yet another application, well-logging, modern drilling tools, also known as down-hole tools (schematic view shown in Figure 2) use electronics to log data real-time on drilling sites. These tools allow the wellsite team to "see" into the rock or earth formations from all angles – up, down, right and left – and gather information that will ensure quick evaluation of the formation prior to invasion. Measurements include resistivity, bit inclination, shock, pressure, temperature, orientation, and magnetic strength. Data is sent to the ground base station via mud telemetry.

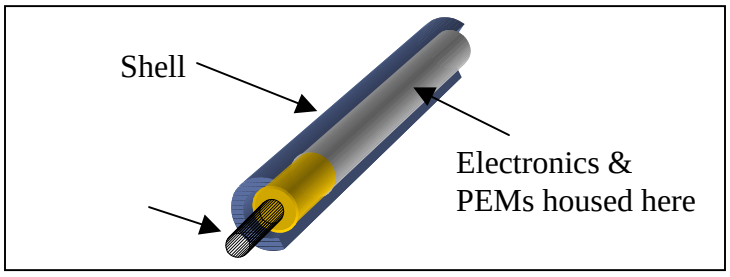

Figure 2: Schematic of Downhole tool

As cabling is not an option due to the long drill lengths and the need for rotation, a distributed system architechture is required. As such, each tool has residing on it sophisticated electronic devices such as field programmable gate arrays, digital-analog converters, digital signal processors, flash memory modules and operational amplifiers.

In oil drilling and geothermal measurement, these electronics can be subjected to extremes of temperature, pressure, acceleration, vibration and corrosion. An example of load conditions to be expected is shown in Table 2. The packaging of the devices such as those mentioned above becomes an immediate concern due to the high temperatures and corrosive external environment to which the tool is exposed.

Load	Range
Temperature	-20°C < T < 320°C
Gage Pressure	0 Pa < P < 90 MPa
Vibration	10 Hz < f < 1000 Hz
pH	2 – 12
Suspended solids	Upto 300,000 mg/kg

Table 2: Oilfield and Geothermal Services Tool Load Summary [2]

Electronic circuits for well-drilling applications could benefit from the availability, functionality, quality and cost advantages of incorporating plastic encapsulated microcircuits (PEMs) into the moderate temperature range applications such as automotives and avionics, that have a maximum temperature of 200°C. In previous CALCE efforts, however, it was found that PEMs have a markedly lower life span at 180°C than ceramic microcircuits, a situation that is not observed at 155°C. There is a need to understand the failure mechanisms that cause PEMs to fail prematurely when operated at 180°C. One very important feature of the failures observed in earlier studies was the wide variation in life span between different PEMs in the same environment. Some of the more complex devices such as microprocessors had a much shorter lifespan than other simpler devices, whose lifespan approached that of ceramic ICs. Furthermore, size and complexity was not the only cause for variation, even devices of similar

complexity and size displayed substantial variation. Possible causes of this variation included concentration of corrosive chemical species in the mold compound, stress levels due to different wirebond geometries in different packages and junction temperature variation due to diffrences in power dissipation among others. Analysis of the failed PEMs revealed that the primary failure mode is the weakening of wirebonds due to intermetallic growth and corrosion of intermetallics at the Au wire to Al bondpad interface. The corrosion was believed to be catalyzed by Br and Sb compounds emitted from flame-retardants in the encapsulant.

Thus, the focus of this work has been to characterize this failure mechanism and to investigate new packaging materials for PEMs to mitigate this failure mechanism.

Wirebonds

Wirebonds are the most commonly used technique for first level interconnect in Plastic Encapsulated Microcircuits (PEMs) (Figure 3).

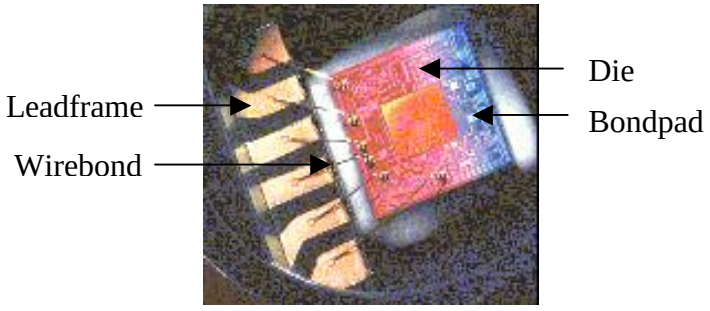

Figure 3: Wirebonds connect the die to the outside of the package

The technique for gold wirebonding in PEMs uses a combination of heat, pressure and/or ultrasonic energy to produce the bond . In the wirebonding process, a high bonding force can lead to material deformation, breaking up of any contamination layer and smoothing out surface asperity, but may also damage the silicon. This process can be enhanced at lower bonding energy by the application of ultrasonic energy. Heat can also improve the bonding by accelerating inter-atomic diffusion and thus, bond formation.

The two major types of wirebonds are ball bonds (Figure 4) and wedge bonds (Figure 5).

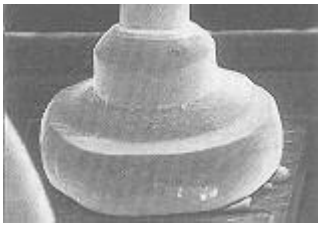

Figure 4: Ball Bond

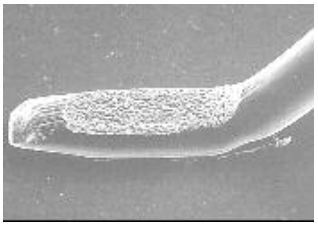

Figure 5: Wedge Bond

Ball bonds are made between gold wire and aluminum bondpads. Wedge bonds are made between the gold wire and the copper leadframe or between Al wire and either Al bondpads or metal leadframes. Al wire cannot be ball bonded.

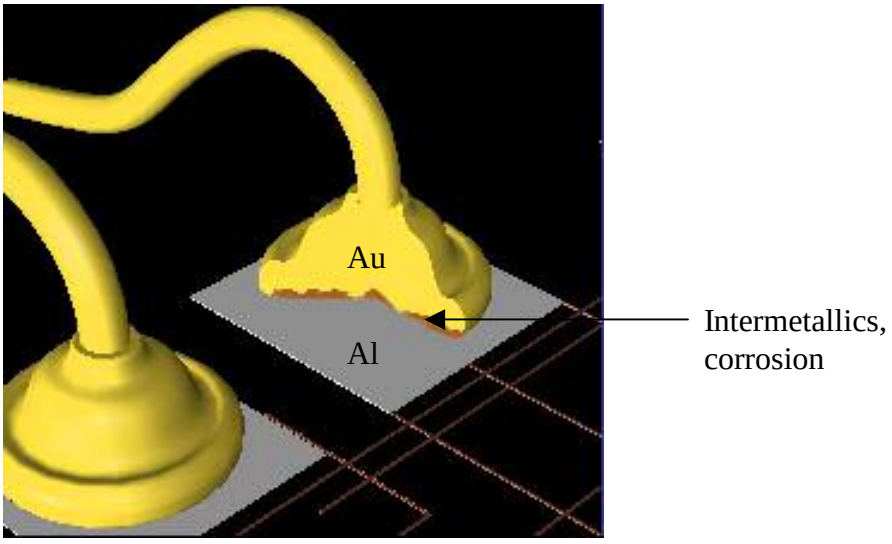

Figure 6: Cross-sectional view of a wirebond showing intermetallic formation

A major reliability issue with gold-aluminum ball bonds is the formation of intermetallics and associated Kirkendall voids (Figure 6) at high temperatures. The formation can be accelerated with operating temperature and time. There are five intermetallic compounds formed: Au_5Al_2 (tan), Au_4Al (tan), Au_2Al (metallic gray), AuAl (white), and $AuAl_2$ (deep purple). At 400°C, Au_5Al_2 and $AuAl_2$ are the first ones to nucleate. Au_5Al_2 grows rapidly at the gold-rich wire side whereas the growth of $AuAl_2$ is extremely slow at the Al-rich bondpad side. The nucleation of the other intermetallics is in the order: Au_2Al (3 minutes), AuAl and Au_4Al (90 minutes) [5]. At lower temperatures, the same order is followed, but it requires more time. Nevertheless, this system often presents a reliability concerns at temperatures above 150°C.

The shear strength of gold-aluminum bonds has been found to be the highest just after fabrication. This is due to the initial interdiffusion and formation of some intermetallic, which strengthens the bond between the two elements. But continued interdiffusion with time and high temperature causes voiding to occur, due to non-uniform diffusion rates of atoms between the gold and aluminum. This voiding, combined with the continued formation of brittle intermetallics can cause crack initiation and propagation through the intermetallics leading to failure. Further complications can arise when corrosive compounds such as bromide ions travel to the site of intermetallic formation, reducing the strength of the already weak wirebond by corroding the intermetallics. These chemicals are present in the flame retardant additives in the molding compound.

In recent years, environmental considerations have led to the trend in the semiconductor industry to promote the use of non-halogen flame-retardants in molding compounds. There are several reasons for this.

Antimony trioxide is possibly carcinogenic to humans (Class 2B) [6]. Bromine is expected to be toxic to aquatic life and expected to adversely affect the ozone layer when released in to the air [7]. It is also bioaccumulative. The European Restriction on Hazardous Substances in Electrical and Electronic Equipment (RoHS) has therefore called for a ban on all brominated flame-retardants by 2006. This is driving the search to find alternatives to these conventional flame-retardants, which may have the fortunate consequence of improving high temperature reliability.

The focus of the study is to characterize the Br-related wirebond weakening process and to establish the high temperature reliability of halogen-free molding compounds.

2 Background – Flame Retardants and the traditional Bromine/Antimony System

Mechanism of Flame Propagation and Retardation

Flame-retardants act physically or chemically in a number of ways to stop flame propagation. The mechanism of flame retardancy is classified into two main categories:

- Physical
  - Cooling: The additives cool the substrate to a temperature below the combustion temperature (e.g. Alumina Trihydrate)
  - Formation of Protective Layer: A solid or gaseous protective layer is formed, keeping out the oxygen necessary for the combustion process (e.g. Phosphorus compounds)
- Chemical
  - Reaction in Gas Phase: The additives interfere with the combustion process by preferentially reacting with free radicals (e.g. Traditional Bromine-Antimony system)
  - Reaction in Solid Phase: The additives react to form a carbonaceous layerBy forming carbonaceous layer on the polymer surface (e.g. Phosphorus)
  - The additives undergo an endothermic dehydration reaction giving off water and causing heat absorption (e.g. metal hydrates like $Al(OH)_3$)

Combustion requires a fuel, an ignition source and oxygen, and can be stopped by removing any of the three. Combustion is initiated by heating a plastic material to its decomposition point. The three critical sources required to sustain combustion process are ignition source, fuel and oxygen. Numerous combustible decomposition products like hydrocarbons, hydrogen and carbon monoxide are formed during branching reactions. Combustion then occurs according to the following reactions 11 [8]:

RH	→ R* + H*	(Initiation)	1
H* + O_2	→ HO* + O*	(Branching)	2
2HO* + CO	→ CO_2 + 2H*	(Propagation, highly exothermic)	3

Solid materials do not burn directly; they must first be decomposed by heat (pyrolysis) to release flammable gases. Visible flames appear when these flammable gases burn with the oxygen (O_2) in the air. The gas flame itself is maintained by the action of high-energy “radicals” (that is H* and OH* in the gas phase) which decompose molecules to give free carbon which can react with oxygen in air to “burn” to CO_2, generating heat energy.

Traditional falme retardant systems use bromine and antimony oxide to stop combustion of the molding compound via a chemical mechanism. The hydrogen and hydroxyl free radicals formed by breaking of chemical bonds in the polymer at high temperatures are the fuel for the combustion process.

RX	→ R* + X*	(Releasing of halogen free radical, high energy)	4

$X^* + RH \rightarrow R^* + HX$ (Reaction with flammable gases, RH) 5

$HX + OH^* \rightarrow H_2O + X^*$ (Reaction with high energy hydroxyl radical) 6

Halogenated flame-retardants attack the flame at this stage, by interrupting the radical release mechanism in the gas phase. When exposed to temperatures above 125°C, the flame retardant molecule releases bromine as a free radical, which reacts with hydrocarbon molecules (flammable gases) to produce HBr. This then reacts with the high-energy H* and OH* radicals to give water and the much lower energy Br radical, which is then available to begin a new cycle of H* and OH* radical removal. The exothermic processes are thus stopped, the system cools down, and the supply of flammable gases is reduced and eventually completely suppressed. Thus, the efficiency of the polymer plastic system depends not only on the bromine content but also on the molecule to which bromine is attached. The chemistry of the system will govern as to when it will start trapping the high-energy free radicals. The effectiveness of the halogen action depends also, very strongly, on the control of the halogen release. Because chlorine is released over a wider range of temperatures than bromine, it is then present in the flame zone at lower concentrations, and so is less effective. Bromine is released over a narrow temperature range, thus resulting in optimal concentrations in the flame zone [9].

Antimony trioxide shows no flame-retardant action on it's own. However, it exhibits a synergistic effect with halogen containing compounds. It acts as a catalyst, facilitating the breakdown of halogenated flame retardants to active radicals. It also reacts with the

halogens to produce volatile antimony halogen compounds, which are themselves directly effective in removing the high energy H* and OH* radicals which feed the flame phase of the fire, thus reinforcing the flame suppressing effect of the halogenated flame retardants. Eqn.s 7-10 show the synergistic effect of antimony oxide [8].

$Sb_2O_3 + HBr \rightarrow 2SbOBr + H_2O$ (~250 °C) 7

$5SbOBr \rightarrow Sb_4O_5Br_2 + SbBr_3$ (245 – 280°C) 8

$4\ Sb_4O_5Br_2 \rightarrow 5\ Sb_3O_4Br + SbBr_3$ (410 – 465 °C) 9

$3Sb_3O_4Br \rightarrow 4Sb_2O_3 + SbBr_3$ (475 – 495 °C) 10

The antimony trihalides and various antimony oxyhalides thus generated act as radical interceptors like HCl or HBr.

The Wirebond-Bondpad Interface

Outgassing of bromine from the mold resin at high temperatures causes corrosion of intermetallics formed at the gold wirebond – aluminum bondpad interface. This causes the interface to degrade further, lose bond strength, increase in electrical resistance and become unreliable. Some of the major issues involved in analyzing this phenomenon are:

- Dependence on temperature
- Rate-limiting step and dependence on concentration of species

The major causes of failure at the bond interface are intermetallic formation and corrosion:

a) Intermetallic Formation

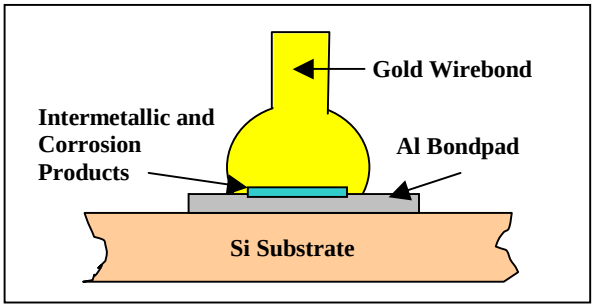

Figure 7: Schematic of bond-pad interface [10]

The structure of the Au-Al wirebond-bondpad interface is illustrated schematically in Figure 1. It shows the site where there is a possibility of formation of intermetallics. Formation of Au-Al intermetallics becomes relevant to the life of a wirebonded PEM only beyond 150°C [3]. So, only such temperature ranges are studied. Philofsky [3] found that the intermetallic formation is mainly composed of gold-rich intermetallics, such as Au_5Al_2 and Au_4Al due to the characteristics of the interface, which contains larger quantities of gold. It was also found that the rate of formation follows a parabolic law, with the initial rate constant (when there is sufficient supply of gold and aluminum) given as: $k = 5.2 \times 10^{-4} \exp(-15900/RT)$ cm^2/sec

b) Corrosion

Corrosion is known to be a reaction of the Au-Al intermetallic compounds and components of the molding compound. After conducting experiments on outgassing in

mold compounds, Thomas et al. [11] proposed that at 200°C, a chemical attack by halogen containing gases on the intermetallic structure initiates a growth change in the structure and leads to excessive bond degradation. Commonly used molding compounds contain flame retardants such as bromine and antimony trioxide. While these are essential parts of the molding compound, they have been found to decrease the reliability of the Au-Al interface at high temperatures.

Kinetics of Corrosion:

High temperature corrosion is understood to follow these steps:

1. Resin Decomposition
2. Bromine Diffusion
3. Intermetallic Formation
4. Chemical Reaction

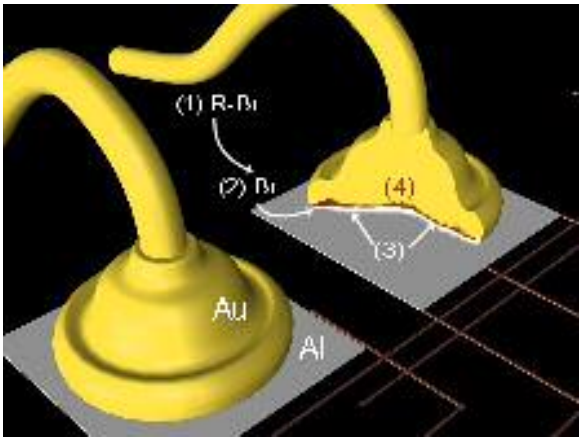

Figure 8: Corrosion Mechanism

Each of these steps has an associated reaction rate and the overall rate of bond failure would be that of the rate-determining step.

The following chemical equations outline the corrosion process leading to bond degradation [11].

$Al(OH)_3 + X^- \rightarrow Al(OH)_2X + OH^-$	Depassivation	11
$Al + 3\ X^- \rightarrow AlX_3 + 3e^-$	Electrolytic Metal Attack	12
$RBr \rightarrow R + Br^-$	Thermal Dissociation	13
$RH + Br^{\cdot} \rightarrow R^{\cdot} + HBr$	Organic Halide Release	14
$HBr + H_2O \rightarrow Br^- + H_3O^+$		15
$AlX_3 + RBr \rightarrow R^+ + [AlX_3Br]^-$	Organic Halide Release	16
$[AlX_3Br]^- \rightarrow AlX_3 + Br^-$		17
$Mau + nAl \rightarrow Au_mAl_n$	Intermetallic Formation	18
$Au_mAl_n + H_3O^+ \rightarrow mAu + nAl^{3+}$	Intermetallic Corrosion	19
$Al^{3+} + 4X^- \rightarrow [AlX_4]^-$		20
$[AlX_4]^- + H_2O \rightarrow Al(OH)_3 + HX$		21
$HX + H_2O \rightarrow H_3O^+ + X^-$	Halide Regeneration	22
$[AlX_4]^- \rightarrow AlX_3 + X^-$	Halide Regeneration	23

The first reaction (Eq. 11) involves depassivation of the oxide layer as proposed by Paulson et al. [13] . $AlBr_3$ is then generated by electrolytic metal attack. $AlBr_3$ is an active catalyst for reaction (Eq. 16) leading to the release of bromide (Eq. 17) from an

alkyl group. For an aromatic group, bromide ions are released by thermal dissociation (Eq. 13), followed by radical reaction (Eq. 14) and hydration (Eq. 15). The hydronium ion produced is the active species that reacts with the intermetallic (Eq. 18) to form gold precipitates and the aluminum cation. Reactions (Eq. 18) to (Eq. 20) show the oxidation of Au_4Al and Au_5Al_2 with Au precipitation. Halide and hydronium ions are regenerated in reactions (Eq. 21) and (Eq. 22).

Khan et al. [14] conducted high temperature tests of prepared samples with bonds coated with a two types of films of brominated resin, and found that the diffusion of Br^- ions out of the resin matrix into the resin metal interface is the crucial rate-determining step, with an activation energy of 0.3 eV. Later studies by the same authors [11] have shown that the original activation energies were much lower due to a high amount of free ionic bromides. In their newer study, materials free from contamination by inorganic salts were found to have activation energies of around 0.7 to 1.0 eV. These activation energies agree with the findings of Gale [15], who has reported an activation energy of 0.8eV for bond degradation.

In experiments performed on commercial MOS devices, Imasato et al. [16] found that the failure rate had an activation energy of 1.14 eV, similar to the Au-Al intermetallic growth, and concluded that (Eq. 18) was the rate determining step.

Uno et al. [10] tested wirebonds encapsulated in two major commercial molding compounds, o-Cresol Novolac (OCN) resin and Biphenyl (BP) resin. They conclude that

the activation energies of the growth of corroded layers on Au_4Al were nearly the same as those of bond failure, and the limiting step is the process of resin dissociation or transportation of reactive bromine gases, which is the same conclusion as that of Khan et al. But the activation energies reported by Uno et al. in their study are quite different. For temperatures greater than 450K (177° C), activation energies are reported as shown in Table 3.

	BP Resin	OCN Resin
Growth of Corroded Layer	1.6eV	2.3eV
Bond Failure	1.8eV	2.3eV

Table 3: Activation Energy Comparison

Khan et al. used varying resins, Imasato et al. tested samples with prepared Au_4Al layers, and Ahmad et al. [17] studied varying Br concentrations, but the study of Uno et al. has been the most comprehensive thus far, combining all the testing done previously.

Corrosion due to high moisture-aging of devices is also possible. Gallo [18] found that antimony trioxide is a major factor in most molding compounds in causing high-moisture degradation while conducting experiments with commercial dies and molding compounds with controlled levels of antimony trioxide.

Brominated compounds dominate degradation at high temperatures, with reactions able to proceed even with comfortable humidity levels, whereas antimony oxides dominate high-moisture degradation at lower temperatures. This may be due to scant quantities of extractable bromine at low temperatures and non-mobility of antimony ions under dry conditions respectively.

Observations and Effects of corrosion:

Corrosion results in the following effects:

a) Decrease in bond shear strength.

b) Increase in electrical resistivity.

c) Decrease in bond pull strength.

Uno et al. used both (a) and (b) do determine failure. Imasato et al. have used (a) in their analysis. Gallo has used (c) to determine the effect of antimony trioxide on moisture-induced corrosion.

Further, Scanning Electron Microscopy (SEM) has been used consistently, to determine qualitatively, the content of the corrosive products, and their spatial location. Gallo has used the SEM to show that antimony is present in largest quantities near the aluminum bondpad base, lesser near the Al-Au interface and none at all in the bulk gold.

Prevention Methods:

Bromine reactions at high temperature cannot be suppressed to improve wirebond reliability, since those reactions are vital for the flame retardancy process. Thus, the prevention methods have to follow a different line of approach. Preventing corrosion can be classified under the following:

Use of ion scavenging chemicals

Gallo has conducted tests with ion scavenging additives and found that they perform better than compounds with no additives under autoclave conditions of high moisture.

But Uno et al. state that in spite of the existence of free-Br trapping chemicals such as $Bi(OH)_3$, it may be difficult to improve reliability of the bonds under dry conditions at high temperatures without changing the physical properties of the molding compound itself.

Elimination of antimony and bromine compounds

Sumitomo Corp. has developed new molding compounds with little (EME HFLS) or no (EME MAR) flame retardants. These are being tested at the CALCE Electronics Center, University of Maryland for high temperature reliability and suitability for PEMs being used in high temperature applications. There may be other issues in the low flame retardant compound such as shorting of adjacent wirebonds by phosphorus, so the recommended molding compound is the flame-retardant-free compound, which uses a smothering mechanism to stop flames from spreading unlike conventional flame retardants, and improves wirebond reliability in the absence of bromine and antimony related corrosion.

3 Background – New Flame Retardants and Alternatives to the Bromine/Antimony System

The major flame retardant alternatives to the bromine-antimony system are:

- Nitrogen-based – Even though the mechanism is not fully understood, they are thought to have several effects [9]:
  - Formation of cross-linked molecular structures in the treated material. These are relatively stable at high temperatures, thus physically inhibiting the decomposition of materials to flammable gases (needed to feed flames – step (1) in Figure 9) .
  - Release of nitrogen gas which dilutes the flammable gases and thus reduces flames.
  - Synergy with phosphorus containing flame retardants by reinforcing their function.
  - The major disadvantage with these compounds is that they have to be used in high concentrations to be effective.

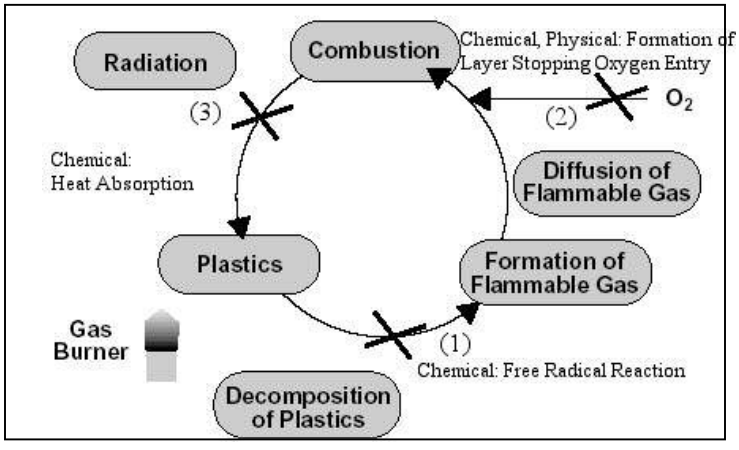

Figure 9: Mechanism of Flame Retardants [19]

- Metal Hydrate [9] –
  - Aluminum trihydrate is decomposed to aluminium oxide around 200°C (which forms a protective, non-flammable layer on the material surface) and water. The water (as steam) forms a layer of non-flammable gas near the material's surface, inhibiting flames. The reaction is endothermic (absorbs heat energy), thus cooling the material and slowing burning.
  - Magnesium hydroxide acts in a similar manner, but is only decomposed at somewhat higher temperatures (around 300°C), meaning that it can be used in plastics which are molded or processed at relatively higher temperatures.
  - These mechanisms of inorganic compounds are however of a relatively low efficiency and the products have to often be used in relatively large concentrations, or more usually, in combination with other types of flame retardants.
  - They also affect the flow characteristics of the molding compound, causing manufacturing issues.

- Metal Oxide [19] –
  - Transition metal oxides promote an insulating carbonaceous layer at the site of combustion (Step (2) in Figure 9).
  - This stops the oxygen from reaching the site and thus stops further flame propagation.

- Although they don’t adversely affect the ball bond of wirebonds in the package, they require good dispersion in the encapsulant medium to achieve an even layer of char while burning.

- Phosphorus-based [9] –
  - Usually act in the solid phase of burning materials.
  - On heating, the phosphorus reacts to give a polymeric form of phosphoric acid (PO3). This acid causes the material to char, inhibiting the “pyrolysis” process (break down and release of flammable gases), which is necessary to feed flames.
  - Vary from elemental red phosphorus (P), which is oxidised to phosphoric acid with heat, through to complex P-containing organic molecules offering specific performance properties.
  - Certain products contain both phosphorus and chlorine or nitrogen, thus combining the different flame retarding mechanisms of these elements.
  - Is found to have high water absorption and poor electrical properties such as shorting, and thus is not a readily acceptable alternative to bromine-antimony.

- Multi-Aromatic Resin –
  - Structure of encapsulant resin used to control the flame.
  - No additives/ flame retardants.
  - Accelerated carbonization (mechanism of stopping the flame is as in Step 2 of Figure 9) or charring due to many aromatic rings in polymer.
  - Easy formation of ‘foaming’ gas due to longer cross-link distance in polymer.

- Has been found by our tests to give superior wirebond reliability at high temperature and high humidity.

Multi-Aromatic Resin

The multi-aromatic resin has been found by high temperature storage and highly accelerated stress tests (HAST) to be a very promising solution to the problem of wirebond reliability at high temperatures. It has fared extremely well in all tests conducted against a low concentration Bromine/Antimony system as a control. The mechanism as described above, is self-extinguishing. The encapsulant has a good flammability rating (on par with conventional encapsulants) and no corrosive chemical behavior. It is currently in production and commercially available.

4 Wirebond Reliability in New Molding Compounds

In this study, an experiment was designed to find the reliability of the gold-aluminum wirebond-bondpad interface in a novel molding compound, and compare it with the interface reliability in a conventional encapsulant, with a typical bromine-antimony flame retardant system.

The two molding compounds used in this comparative study were MAR (multi aromatic resin) and HF (high filler content – same as conventional encapsulant, but with much more filler content (~90%), and very less Br-Sb (less than 1600 ppm) flame retardant). For each compound, 50 Medium Quad Flat Package (MQFP) samples with a 16X24 leadframe were manufactured for testing. The HF samples were the control group.

Three separate experiments were performed on each sample:

1. High Temperature Storage Life (HTSL) – 180°C
2. High Temperature Storage Life (HTSL) – 200°C
3. Highly Accelerated Stress Test (HAST) – 130°C, 85% RH

These experiments were conducted in two parts (A and B) as shown in the following tables:

	Experiment 1	Experiment 2
Conditions	180°C	200°C
HF	5 samples	5 samples
MAR	5 samples	5 samples

Table 4: Part A - Test for Bond Degradation

In Part A, 5 samples were used for each combination (a cell in Table 4) of temperature and molding compound type, giving a total of 5X4 = 20 samples. Among each 5-sample set, the first part was exposed to 50 hours, the second to 100 hours, the third to 200 hours, the fourth to 300 hours, and the fifth to 500 hours. After each sample was taken out, its electrical resistance was measured, and destructive physical analysis was performed on the part. The aim of Part A was to show the wirebond degradation, and the rate at which it occurred.

	Experiment 1	Experiment 2	Experiment 3
Conditions	180°C	200°C	130°C, 85%RH
HF	10 samples	10 samples	10 samples
MAR	10 samples	10 samples	10 samples

Table 5: Part B - Test for Bond Failure Rate

In Part B, 10 samples were used for each combination (a cell in Table 5), making the total number of samples used = 6X10 = 60. Each sample was exposed to 1200 hours in experiments 1 and 2, and 800 hours in experiment 3. Electrical resistance was monitored on 4 chosen sites on each sample at intervals of 50 hours, 100 hours and every successive 100 hours. The aim of Part B was to look at the failure rate using a large sample set of 40 connections and compare the relative failure rate in each type of molding compound.

Sample Description

The samples used in all the experiments were 24X16 pin Medium Quad Flat Packs (MQFPs) with dummy dies. The die is made up of daisy-chained metallization lines, like a standard die. The Au-Al wirebond-bondpad connections are also typical of PEM packages. Not all bondpads are bonded. There are 8 pairs (16 wirebonds) coming out of

the die at selected points. The electrical path across each pair is through 2 gold-aluminum interfaces and one short metallization strip.

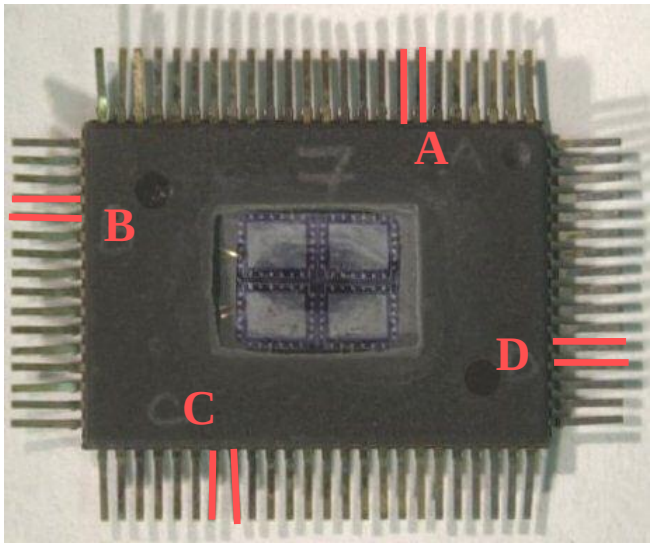

Figure 10: Decapsulated Sample Photograph

Figure 10 shows a photograph of a decapsulated sample, with the die exposed. A few wirebonds can also be seen (shining, on left side). The sites chosen for resistance monitoring are labeled A,B,C and D. They are the first of the two connection pairs on each side taken clockwise from the indentation on the top right. Thus, A is the connection across pins 7 and 8 counted from the right on the top side of the package in Figure 10, and so on.

Die detail is shown in Figure 11. The electrical connection across each set of terminals is a small metallization strip. On the die are other metallization lines connecting peripheral bondpads, which are not used in the current experiment.

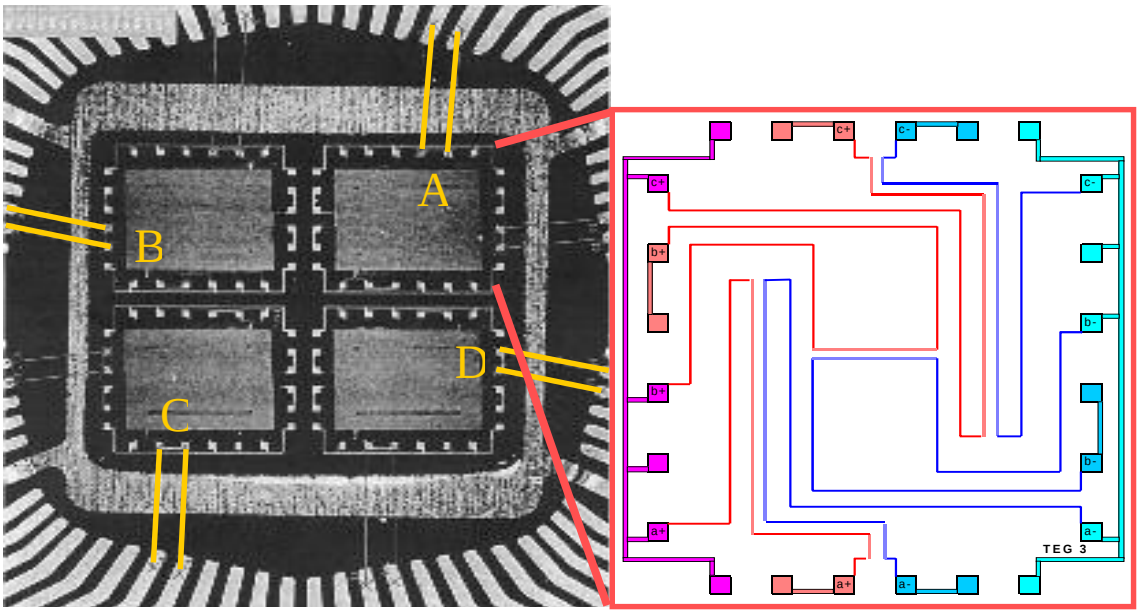

Figure 11: Die Detail

Hardware

The high temperature storage life tests were performed in a --- environmental chamber and the highly accelerated stress tests were performed in a --- chamber. HP3490A data acquisition units were used to monitor case temperature continuously in the high temperature chambers. Electrical resistance was monitored manually using the same data acquisition unit at periodic intervals (50 hours, 100 hours and every successive 100 hours). Figure 12 shows the schematic view of the experimental setup in each high temperature chamber. Figure 13 shows the actual experimental setup and the environmental chamber, with the data acquisition unit on the lower right of the image.

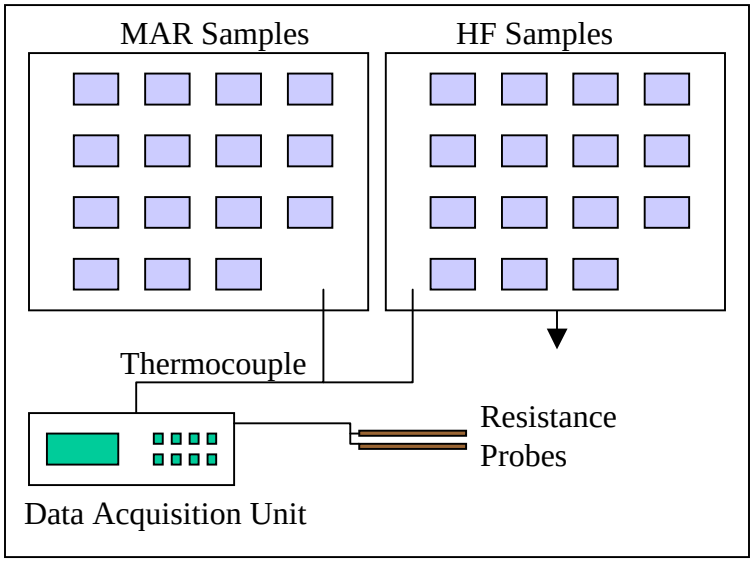

Figure 12: Schematic of experimental setup

The components were placed on an aluminum sheet (Figure 12) with holes. This provided airflow around the component, and ensured that the component was heated uniformly and with minimum rise time.

Figure 13: Experimental Setup

Failure Analysis

The failure analysis techniques were chosen to find causes of failure and rate of failure of the wirebond-bondpad interface. The primary failure analysis techniques used were:

a) Electrical resistance measurement

A HP 34901A 20-channel multiplexer was configured with an Agilent 34970A data acquisition unit to measure the resistance using a 4-wire measurement technique, to get resistance values accurate upto 0.01Ω. This accuracy was needed since the initial resistances were around 0.85Ω, and the initial (first few 100 hours) resistance changes were of the order of 0.1Ω. The 4-wire method eliminates resistance of the leads, and contact resistance. So, electrical failure could be determined accurately. The principle of 4-wire measurement is to force a current through the load resistance by using one pair of wires from a current source and to sense the voltage across the same load resistance using another pair of wires as a voltage sense. The voltmeter which senses the voltage has a very high internal resistance, so no current flows through the sense wires. Manual measurement produced a non-repeatable resistance values well beyond electrical failure as defined by the manufacturer (1.2 times initial resistance). This could be due to manual stressing of the leads while measurement, making or breaking partial contact, resulting in resistance swings. Such swings started only after 2Ω. Below 2Ω, all the resistance measurements were repeatable, even though electrical failure (around 1.1Ω) was reached well before 2Ω. The value chosen as the failure criterion for statistical data in Part B of the experiment (as explained before) was 2Ω, since it was below repeatable limits, and

also gave a good failure distribution, as opposed to 1.1Ω, which would have indicated failure for all parts very early, and it would not have been possible to compare slopes.

Further, the electrical resistance was taken, for each sample type, as an average of 60 connections at 50 hours, 56 connections at 100 hours, 52 at 200 hours, 48 at 300 hours and 44 at 500 hours. The reason for this is that resistance measurements were made for all samples, but the samples in Part A of the experiment were to be exposed only to fixed time periods, and had to be taken out at predetermined intervals. The large number of connections gave a good statistical sample set, and were also found to agree with the other methods of failure analysis, as will be shown later, suggesting that the method of manual measurement with a 4 point probe was justified, and unwanted errors due to oxidation of leads, external lead resistance etc. were not included.

b) Decapsulation with fuming HNO_3

After the electrical measurement, the samples had to be exposed for destructive analysis. Decapsulation was carried out with the B&G Decapsulator model 250E. Fuming HNO_3 was used to expose the die area. Decapsulation times were higher for parts stored at high temperature for longer time, and the decapsulation time varied from 35 seconds to 140 seconds. Etch temperature was set at 85°C. After acidic etching, the component was rinsed with acetone and air-dried.

c) Microtesting (Bond Shear)

Bond shear testing was performed on the samples immediately after decapsulation to find the shear strength of the wirebond. Testing was done on a Dage BT4200 with a BS200gm load cell. After cleaning the surface of the die with and air jet, the shear tool is placed adjacent to the wirebond and force is applied on the bond by the tool till it doesn't receive a resistance (full bond shear). A stand-off height of 0.4 μm was used. If the surface is not properly cleaned, the bond shear machine encounters irregularities and aborts the test. Thus, it is important to decapsulate and clean the die surface properly. Care must be taken not to touch the bonds or reduce their integrity while cleaning. This test is done to determine ball bond integrity.

d) Microsectioning

Cross sectioning was done on the samples to determine extent of intermetallic growth or corrosion growth at the ball bond to bond pad interface. The samples were repotted in an epoxy compound with 10:3 resin:hardener ratio. The re-encapsulation was done to have support for the fragile wirebonds and die while sectioning them. After the epoxy hardened, the samples were ground until the required interface was reached. Grinding was done in stages, with decreasing grit size SiC paper. The grades sizes used, in chronological order, were 240, 400, 600, 800 and 1200. A final polish was done using 0.3 μm Al_2O_3 powder, 0.05 μm Al_2O_3 powder, and 0.05 μm colloidal silica.

e) Scanning Electron Microscopy

A Scanning Electron Microscope (SEM) was used to study the morphology and composition of the test samples. The benefits of the SEM over conventional microscopy

include very high resolution and a greater depth of field, which is especially useful in the 3-d images of the wirebonds as shown in Table 8. A focused beam of electrons hits the sample at the site of inspection, and the electrons emitted from the specimen (secondary and backscattered) are collected by sensors to produce a magnified and detailed image. Secondary electrons are low energy electrons ejected from the sample as a result of inelastic collisions with beam electrons. They are produced near the surface of the sample, from a small area around the beam tip. The resolution of the image is therefore very good because the beam is only a few nanometres in diameter. Backscattered electrons are primary electrons emitted as a result of elastic collisions with specimen electrons. BSE emission intensity is a function of the specimen's atomic number; i.e., the higher the atomic number (e.g., Fe(26) vs. Mg(12)), the brighter the signal.

The SEM can also be used to perform qualitative microanalysis. For examples, it was used to determine quantities of Al, Au and O at different sites on the sample. When the beam interacts with the sample, energy is released in the form of radiation over a variety of wavelengths. This energy results from beam electrons ionising the inner electron shells of an atom. When the excited atom relaxes, i.e., an outer electron filling the inner shell, radiation is released which is characteristic of the atom's electron shell’s energy. Using the energy to demarcate the elements is called Energy Dispersive Spectroscopy (EDS), whereas using the wavelength to demarcate the element is called Wavelength Dispersive Spectroscopy (WDS). WDS was used in this work, since energy levels of Bromine were too close to Aluminum, and both elements were present in the samples studied.

Results – Part A

HF compound:

A study of the average electrical resistance shows that the resistance increase is gradual at 180°C, as seen in Figure 14, and it crosses the failure value of 2Ω around 300 hours. This agrees with the bond strength gradually decreasing before 300 hours and dropping to much lower levels between 300 and 500 hours as in

Figure 15. Further, it also agrees with intermetallic growth data in Figure 16, which show the gradual growth and saturation of the intermetallic corrosion layer. At 200°C, though, resistance increases rapidly, and complete failure was observed at 200 hours, all circuits were electrically open beyond 200 hours, indicating complete loss of electrical conductivity due to the formation of an insulating corrosion layer. Bond strength also drops rapidly early on as seen in Figure 15, corresponding to electrical resistance and intermetallic growth.

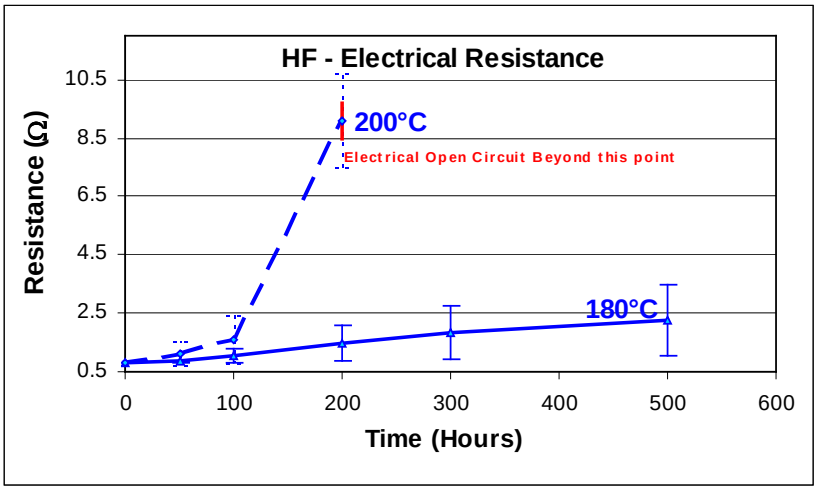

Figure 14: Electrical Resistance in HF

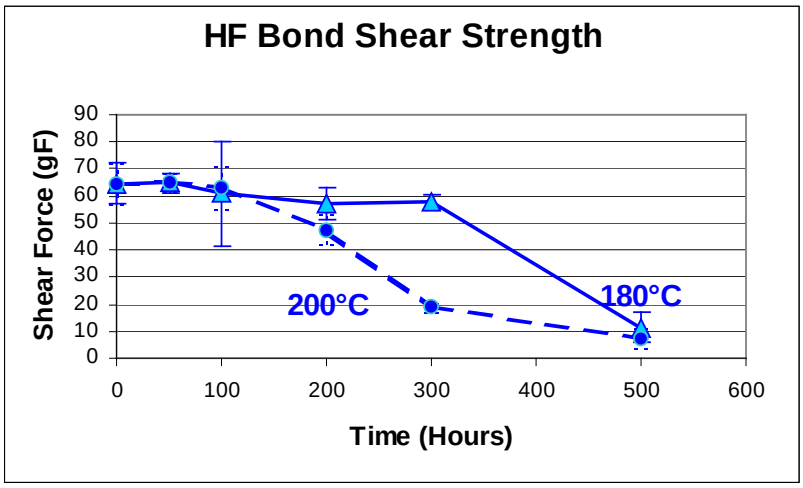

Figure 15: Bond Strength in HF

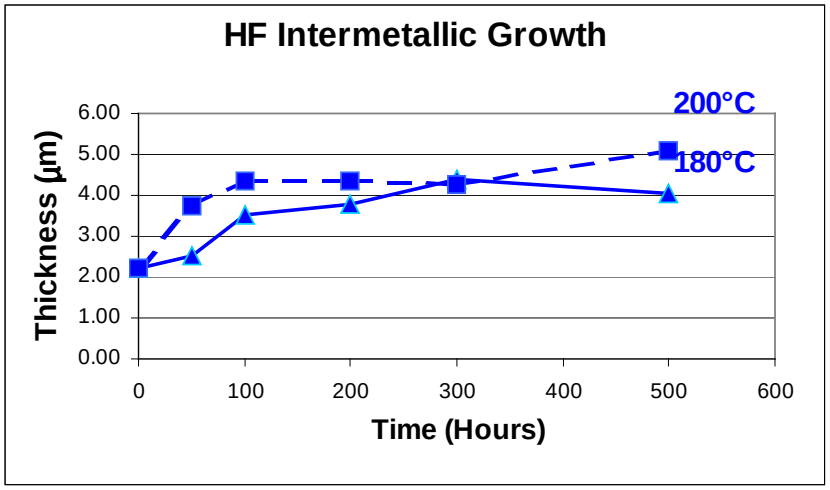

Figure 16: Intermetallic Growth in HF

MAR compound:

In contrast to the HF compound, the wirebond reliability was maintained for a much longer period in the MAR samples. Although the average electrical resistance started to

increase beyond 300 hours at 200°C, it did not go beyond 1.5Ω in the first 500 hours at 200°C, and the average electrical resistance was negligibly higher than the initial resistance at 180°C (see Figure 17). The bond shear results (Figure 18) agree very well with the electrical resistance measurement, showing that at 180°C, there is little change in the strength, but at 200°C, there is a gradual drop in bond strength after 300 hours. Thus, even at 200°C, the wirebonds exhibit much better reliability in this compound.

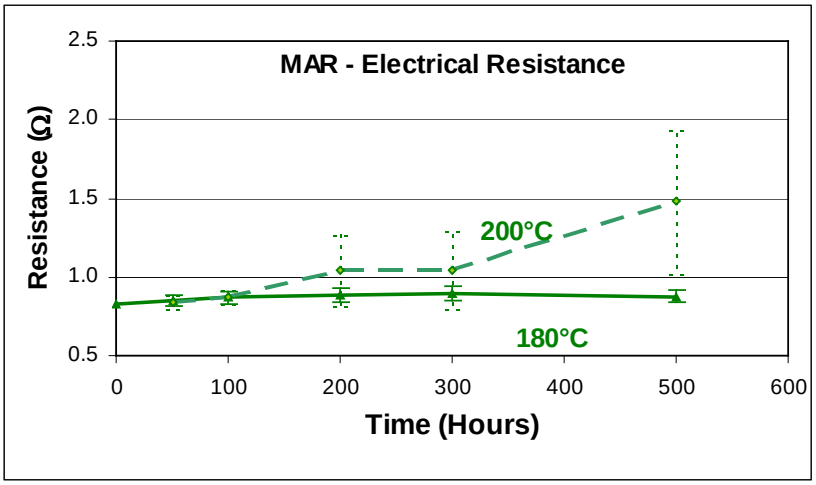

Figure 17: Electrical Resistance in MAR

There is rapid intermetallic growth at 200°C as seen before in the HF compound, and only gradual growth at 180°C, again as seen in the HF compound, but the overall thickness levels are 0.5µm to 1µm lesser than the HF compound. This is attributed to the extra corrosion layer in the HF compound, due to the presence of brominated flame retardants. Although the difference between the layers in the HF and MAR compounds was not apparent in the optical micrographs, the separation of the ball bond from the intermetallic layer was clearly seen in the HF wirebond pictures (as in Table 6). In the MAR compound, extensive voiding and/or loss of contact is not present, since such

events take place only at very high temperatures (around 400°C) due to intermetallic formation alone [3]. Thus, we can only see loss of contact beginning to form as a small crack in the pictures of advanced stages of high temperature (200°C) exposure in Table 7. Further, in the HF compound, the loss of contact started at the edge of the bond and grew inward, suggesting that the bromine also moves in from the edges as the corrosion process continues.

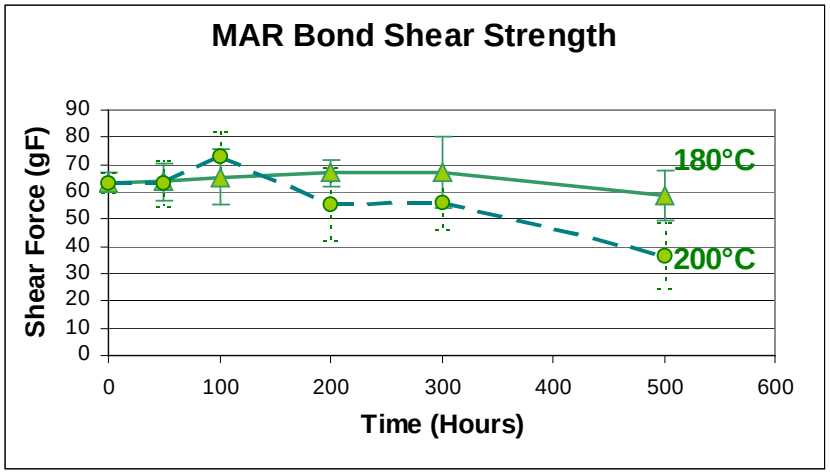

Figure 18: Bond Shear Strength in MAR

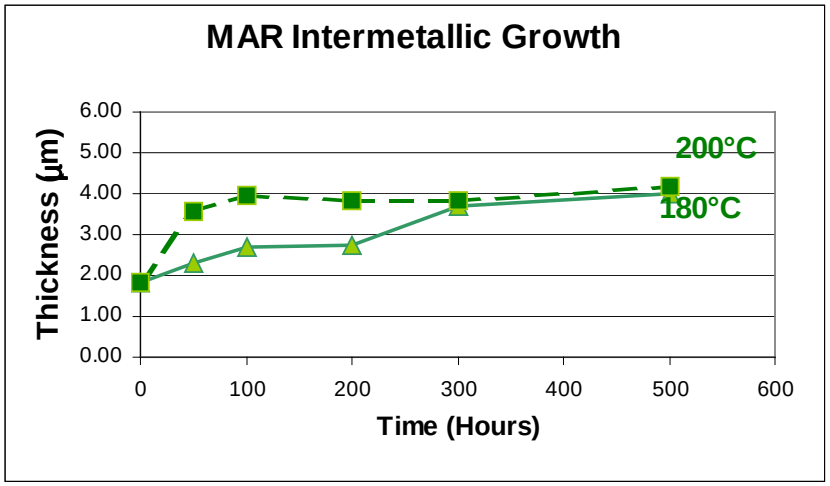

Figure 19: Intermetallic growth in MAR

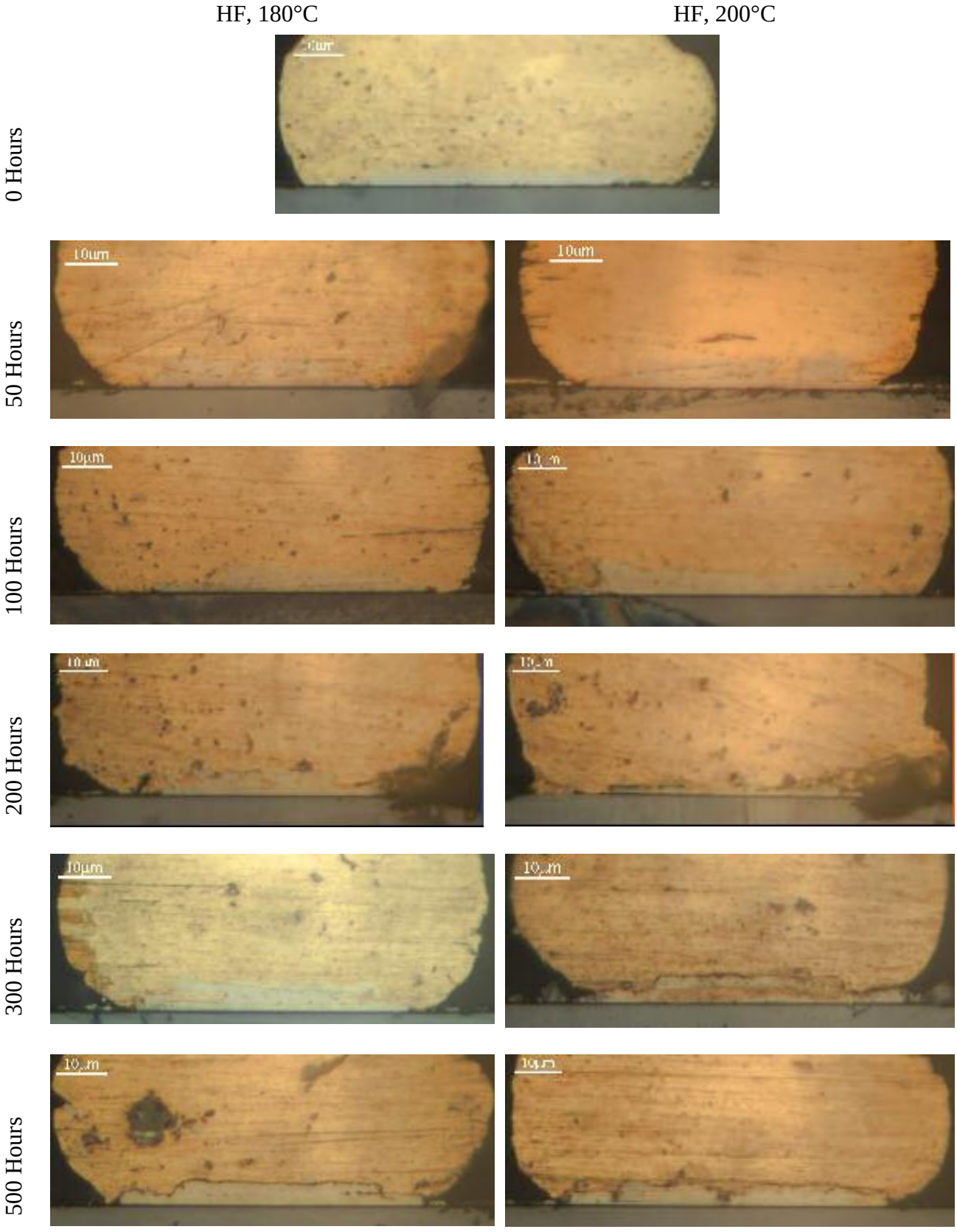

Table 6: Intermetallic Growth in HF

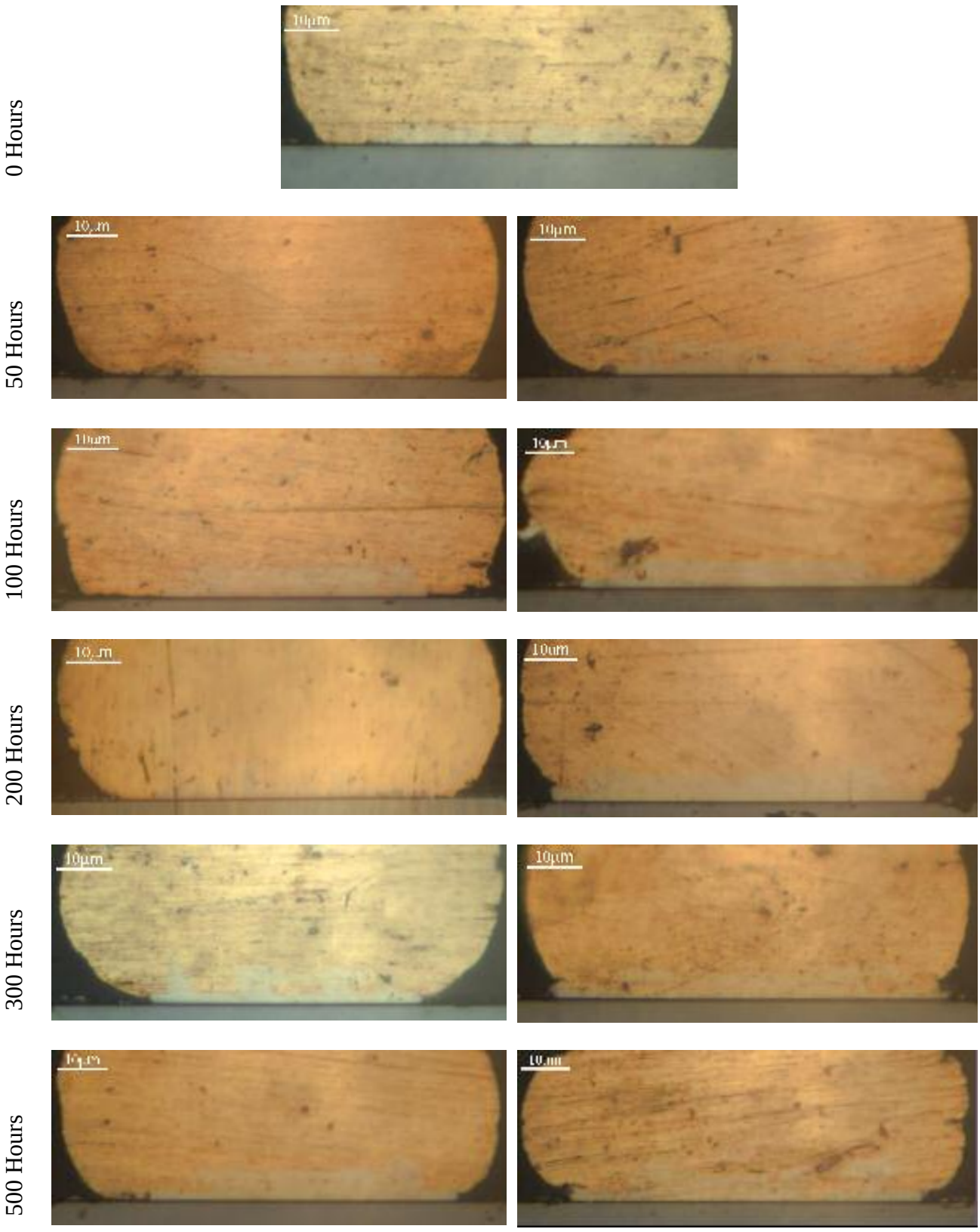

Table 7: Intermetallic Growth in MAR

SEM images of the 4 combinations of conditions and compound type show that corrosion starts early in the HF compound, as compared to the MAR compound.

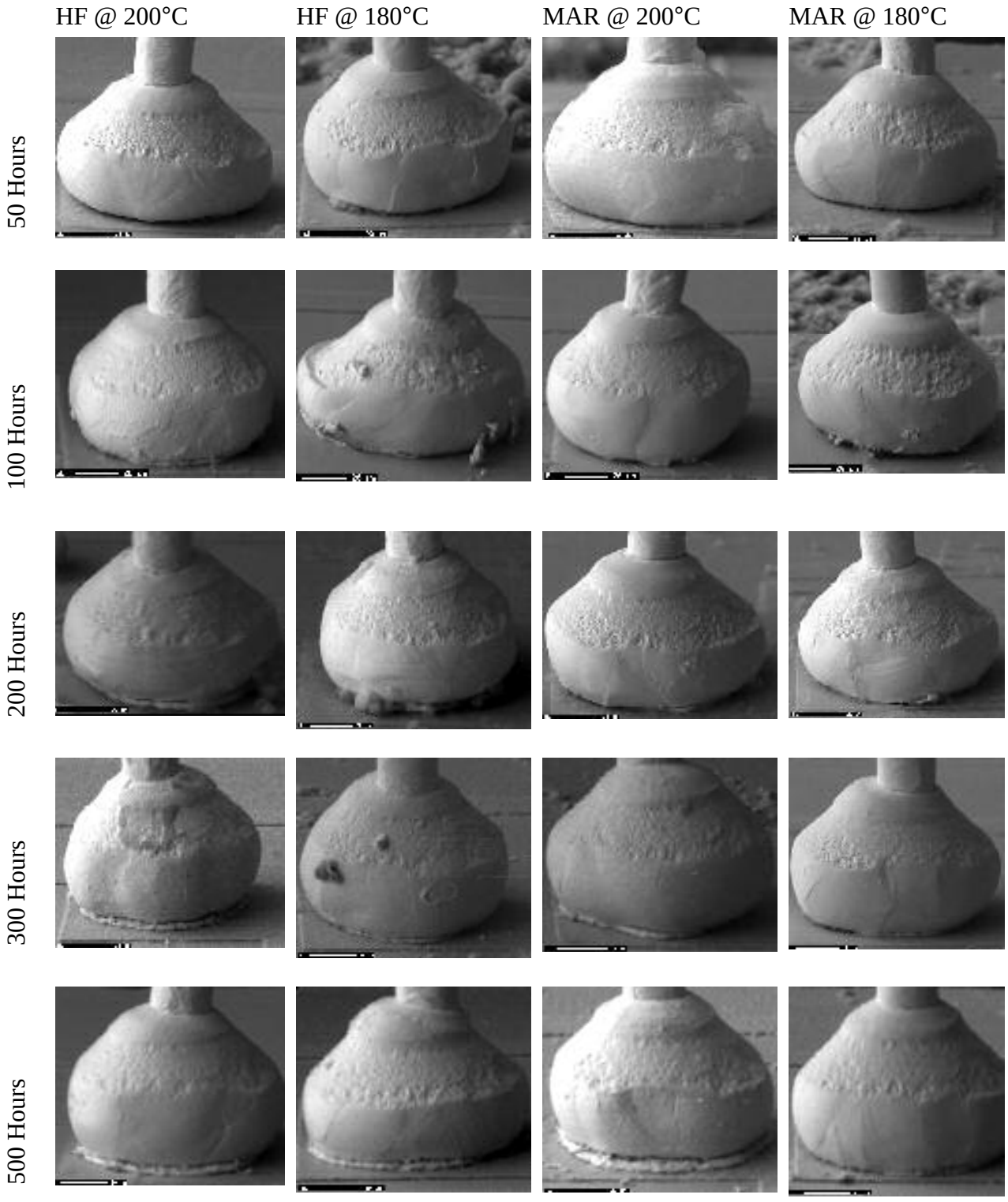

Table 8: SEM Images of the Wirebond

Intermetallic growth in the MAR compound can be seen after 200 hours at 200°C, but intermetallic growth in MAR is minimal at 180°C. The images are arranged worst case to best case wirebond reliability left to right, and increasing exposure time top to bottom.

Results – Part B

The number of failed connections (for resistance above 2Ω, as explained previously) were plotted against the time of exposure (Figure 20). Resistance readings were repeatable upto 2Ω, but were not repeatable beyond 3Ω. Thus, 2Ω was chosen as the failure criterion, since it was the highest repeatable and reliable resistance level, with a guardband of 1Ω from the higher unrepeatable resistance readings. Further, the choice of the failure criterion was based on resistance readings alone, and not on wirebond shear data, since the trend of wirebond degradation could not be seen until the completion of the experiment, whereas the trend in resistance readings could be seen during measurement.

At 180°C, the wirebonds in the HF compound started failing as early as 100 hours, and all bonds filed at 700 hours. Wirebonds in the MAR compound started failing only at 700 hours. The rate of failure for the HF compound shows 2 slopes, the second one larger than the first, with the transition at 500 hours. This could be due to minimal corrosion with intermetallic formation below 500 hours and extensive corrosion after 500 hours. The MAR compound shows only one slope for the duration of measurement, and only intermetallic formation was observed in this compound, suggesting that the slope is an

indication of the rate of failure due to intermetallic formation and voiding due to differential diffusion alone.

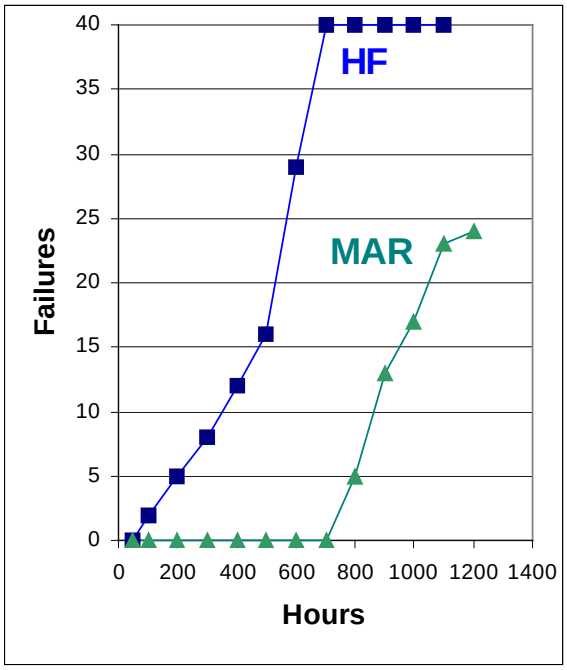

Figure 20: Number of failures at 180°C

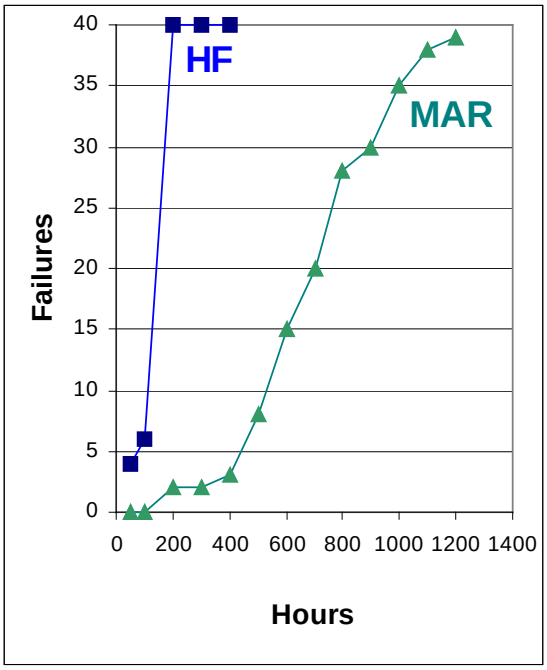

Figure 21: Number of failures at 200°C

At 200°C (Figure 21), similar patterns are observed, but the failures start much earlier. All wirebonds failed under 200 hours in the HF compound, but it took around 1200 hours for complete failure of the wirebonds in the MAR samples. The failure slope in the MAR compound is the same as the one at 180°C, suggesting that the same mechanism (intermetallic formation, and the resulting voiding alone) is responsible for failures. Thus, the MAR compound has shown superior reliability compared to the HF compound at temperatures greater than 180°C.

An observation made in the high temperature experiments of Part B was the behavior of the G700 compound at 180 °C. There was a preferential failure in the following order: C – B – D – A (Figure 22). The pdf (Figure 23) shows that C and B sites had very close distributions, whereas D was farther out, and A had no failures. The trend was reconfirmed during decapsulation, where most of the unetched mold compound was found in A and D. But this preferential behavior was restricted only to the G700 compound at 180 °C. It is possibly due to process factors such as mold compound flow direction.

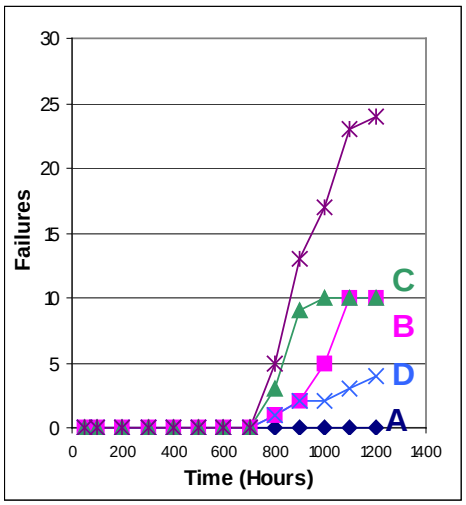

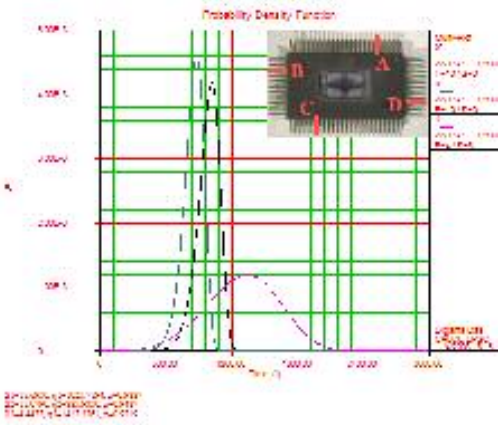

Figure 22: Preferential Failures for G700 @ 180 °C

Figure 23: Failure Distribution (pdf)

Finally, the results of Experiment 3 of Part B (high moisture conditions), as seen in Figure 24 indicate that resistance increases were marginal and total resistance was under 2Ω even at 700 hours. Resistance increase in the MAR compound were negligible, and much lesser than the HF compound. Thus, wirebonds are more reliable in the MAR compound in both high temperatures and high humidity conditions.

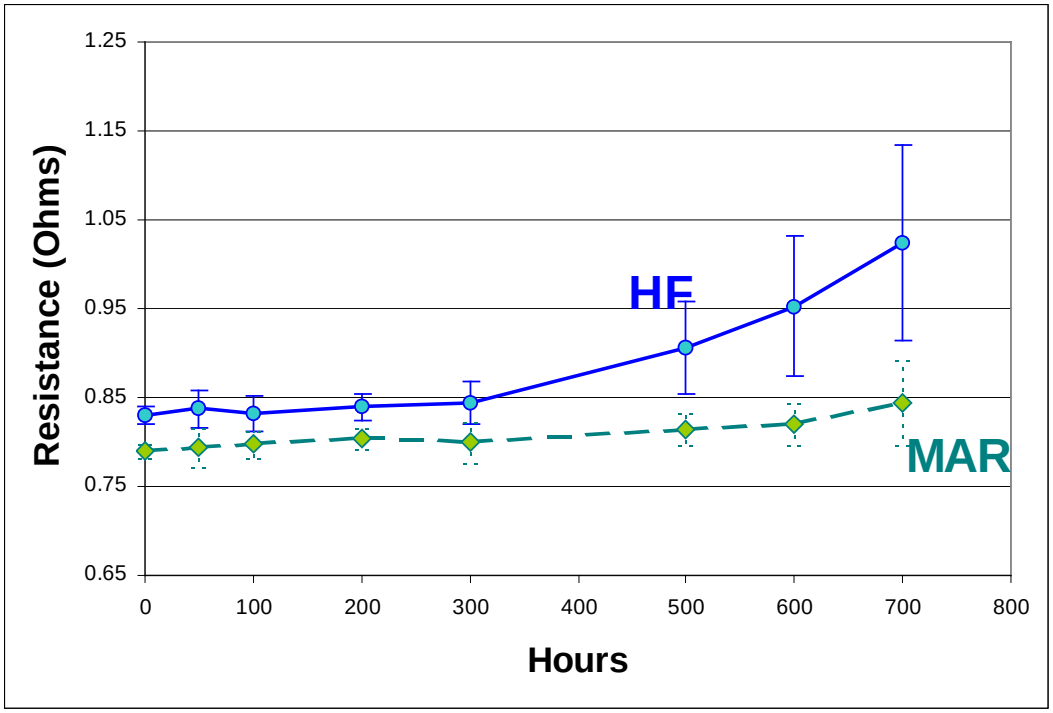

Figure 24: Resistance increase under HAST

5 Characterizing Wirebond Reliability in Conventional Molding Compounds

Commercial plastic packages are mass-produced and customization increases costs. To select the package most suited for the target application, a test plan is required to qualify the package for the specific environment. At the end of the initial part of the study and literature review, the following were identified:

1) Dominant failure mechanism in plastic ICs at 180°C is corrosion of intermetallics at the Au bond – Al pad interface.
2) Chemical reactions that cause bromine to accelerate the corrosion of the Au-Al intermetallics at the interface.
3) The rate determining step is that of bromine transport from the encapsulant bulk to the interface.
4) The encasulant resin has a sizeable effect on the corrosion, since it affects the bromine transport. It has been found that biphenyl based and dicyclopentadiene (DCPD) based epoxy molding compounds have a lower T_g, and thus cause easier transport of bromine than cresol novolac based (CN) epoxy compounds.

Screening Plan

Based on previous research, we have developed a test plan which provides a first-cut assessment of the susceptibility of a PEM to failure by intermetallic corrosion-induced

failure of Au-Al wire bonds, and thereby an assessment of the suitability of a PEM for a high temperature application. This plan includes the following steps:

1) Tests to Determine Concentration of Flame Retardants
2) Procedure to determine the type of encapsulant resin
3) Electrical Tests.
4) Failure Analysis

Each step is described in detail:

1) Conduct tests to determine the concentration of free (hydrolyzable) bromine, total bromine and antimony in the encapsulant.

    a. Antimony content is to be measured using Atomic Absorption Spectroscopy: Atomic absorption spectroscopy (AAS) determines the presence and concentration of metals in solution. This method is highly suitable for antimony measurement in PEMs since typical concentrations in PEMs are in the low mg/l range and the instruments sensitivity is in the ng/l range.

    In their elemental form, metals will absorb ultraviolet light when they are excited by heat. Each metal has a characteristic wavelength that will be absorbed. The AAS instrument looks for a particular metal by focusing a beam of UV light at a specific wavelength through a flame and into a detector. The sample of interest is aspirated into the flame. If that metal is present in the sample, it will absorb some

of the light, thus reducing its intensity. As the concentration increases, the intensity decreases. The instrument measures the change in intensity. A computer system converts the change in intensity into a value for absorbance. The researcher can construct a calibration curve by running standards of various concentrations on the AAS and observing the absorbances. Then samples can be tested and measured against this curve.

To prepare the samples in liquid form, the electronic packages are cut into smaller pieces. Since the molding compound is intimately fused with other parts of the package, it is important to separate stray metal such as copper, nickel and gold from the pure molding compound. To isolate the mold compound sample from the other packaging materials, the center of the package can be cut out with a diamond saw and discarded. The leadframe can be removed by chipping the upper and lower panels of mold compound away from the sandwiched leadframe. If necessary, further isolation of material can be performed magnetically, centrifugally, or by using a fine tweezer to pick out stray particles. If the package is extremely small (less than 4mm on each side and less than 2mm thick), or if large quantities of sample are required, material contamination at the cutting stage is unavoidable and manual separation must be conducted.

The extracted molding compound is then ground into very fine pieces using a ceramic mortar and pestle (which is cleaned with fuming nitric acid and rinsed with deionized water). Depending on the amount of sample available, 1-20 mg is

dissolved in 6-10 ml of fuming nitric acid. The solution is then further diluted with deionized water, the amount of water depending on the sample size. A 1 ml sample of the final solution is used in the AAS instrument. Careful records are kept of the amount of encapsulant dissolved and the dilution ratio to allow proper calculation of the concentration of antimony in the encapsulant from the AAS determined concentration of antimony in solution.

b. Ion Chromatography / Extraction is performed to determine the water extractable (hydrolysable) concentration of bromine in the molding compound. However, this technique was found to give inaccurate results for very small sample weights. Sample extraction is the same as described for AAS. For liquid solution preparation, the molding compound powder is dissolved according to MIL-STD-883, Method 5011.

Ion chromatography is an experimental technique used for analyzing and/or separating mixtures of chemical substances [10]. All chromatographic methods share the same basic principles and mode of operation. In every case, a sample of the mixture to be analyzed (the analyte) is applied to some stationary fixed material (the adsorbent) and then a second material (the eluent) is passed through or over the stationary phase. The compounds contained in the analyte are then partitioned between the stationary adsorbent and the moving eluent. The success of the method depends on the fact that different materials adhere to the adsorbent with different forces. Some adhere to the adsorbent more strongly than others and

are therefore moved through the adsorbent more slowly as the eluent flows over them. Other components of the analyte are less strongly adsorbed on the stationary phase and are moved along more quickly by the moving eluent. So, as the eluent flows through the column, the components of the analyte will move down the column at different speeds and therefore separate from one another. If the end of the columns is monitored, at some point, molecules or ions of the fastest moving substance (least tightly bound to the adsorbent) will be observed to emerge from the column - usually in a narrow band. Shortly thereafter, molecules of the second fastest moving substance emerge from the column and so forth.

c. Total Bromine content is measured using X-ray Fluorescence (XRF). The XRF method is widely used to measure the elemental composition of materials. When a primary x-ray from an excitation source, such as an x-ray tube or a radioactive source, strikes a sample, the x-ray can either be absorbed by the atom or scattered through the material. The process in which an x-ray is absorbed by the atom, transferring its energy to the ejection of an inner-shell electron is called the "photoelectric effect." This process creates inner-shell electron vacancies that present an unstable condition for the atom. To return the atom to its stable condition, electrons from the outer shells are transferred to the inner shells and in the process give off x-rays of characteristic energy equal to the difference between the two binding energies of the corresponding shells. Because each element has a unique set of energy levels, each element produces x-rays at a unique set of energies, allowing one to non-destructively measure the elemental

composition of a sample. The process of analyzing the composition of a sample based on the emission of characteristic x-rays is called "X-ray Fluorescence Spectroscopy." In most cases the innermost K and L shells are involved in XRF detection. A typical x-ray spectrum from an irradiated sample will display multiple peaks of different intensities. [20]

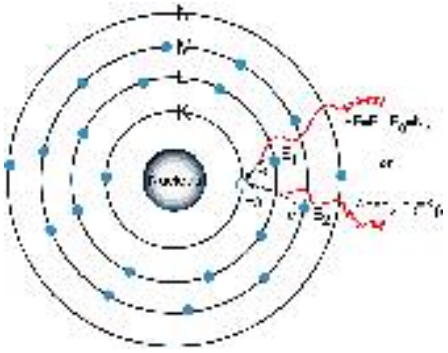

Figure 25: Characteristic X-Ray Emission from K-shell of an Element [20]

Normal sample sizes for XRF spectroscopy are more than an inch in diameter, but due to the small size of the samples in this study, a tin shield with a 0.25-inch diameter hole was used to reduce the incident x-ray beam diameter down to a size that permitted a constant area to be irradiated on all samples. An advantage of this technique is the lack of solution extraction or other sample preparation.

d. Total bromine content can also be measured using wavelength dispersive spectroscopy (WDS). This is similar to XRF except that the excitation source is electrons instead of X-rays. The advantage of this is that electrons can be focused to a much smaller spot size permitting irradiation of smaller areas on the sample. In this technique, a beam of electrons is directed at the sample, the highly

energetic incident electrons knock electrons out of the inner shells of the sample atoms. When an excited atom relaxes (i.e., an outer electron fills the inner shell) X-radiation is released at a set of energies/wavelengths that is characteristic of the atom. If the energy of the X-ray is used to demarcate the elements, the technique is called Energy Dispersive Spectroscopy (EDS), whereas if the wavelength is used to demarcate the element, the technique is called Wavelength Dispersive Spectroscopy (WDS). WDS is preferable for bromine detection, since the energy levels of bromine are too close to aluminum for adequate signal resolution in EDS, if both elements are present, as they are in commercial PEMs.

2) Determine the type of encapsulant resin.

It is important to realize that in this step one is not looking for the complete composition of specific molding compounds, which is often proprietary to the manufacturer, but rather only for the class of molding compound (i.e. epoxy biphenyl, epoxy cresol novolac, DCPD).

a. The first step is to refer to the manufacturer's datasheets for the device, which should be available on the manufacturer's website. In the likely event that the molding compound is not specified on the datasheet, the manufacturer can be directly queried. The queries can be directed to the customer service or applications engineering departments. While the molding compound used for each package is recorded, it is often not readily available to the customer service

personnel and it may take some time to locate the information. In addition, the molding compound may vary from device to device and from lot to lot for a particular device. If the package manufacturer provides only the molding compound code, the molding compound manufacturer can be approached and queried in the same manner about the molding compound type.

b. If part (a) does not produce results, the next step is to use differential scanning calorimetry (DSC) or thermo-mechanical analysis (TMA) to determine the glass transition temperature (T_g), which is a function of the mold compound resin structure. Each type of molding compound has a different T_g. The T_g of biphenyl molding compounds is 10°C-15°C lower than that of epoxy cresol novolac molding compounds.

In DSC, two pans are heated in a computer-controlled furnace. One pan is a reference pan containing a high melting point metal, and the other holds the sample to be tested. The computer plots the difference in heat flow against the temperature. Since polymers have a higher heat capacity above T_g than below it, the T_g can be determined from the point at which the plot shifts downwards.

TMA consists of a small indenter-type probe that is pressed with a small force against the surface of the specimen. Variations in temperature cause the material to expand or contract, thus moving the probe. The position of the probe gives a measurement of the displacement of the material tested and an abrupt change in

the displacement or the rate of displacement of the materials indicates a transition. Thus, a plot of expansion against increasing temperature can be used to determine T_g, as the coefficient (or rate) of thermal expansion of a polymer increases rapidly at the T_g.

Once the bromine and antimony concentrations are known along with the temperature of the molding compound during operation and the resin type, a formula can be used to determine the reduction in bond strength as a function of time. This reduction in bond strength is caused by the formation and corrosion of intermetallics and can be related to the time to electrical failure based on the interaction between the weakening bond strength and the thermomechanical stress imposed on the wirebond during operation by the package. Different constants are used in the formula based on the type of encapsulant, so the encapsulant type must be known so the correct version of the formula is employed.

The following section describes the experiments that were conducted to create a model linking the bromine and antimony concentration and the resin type to the degradation of the bond strength, thus both calibrating and validating this approach to part screening.

Calibration/Validation Example

Samples of each of nine different PEM devices encompassing nine different IC functions were provided for testing. These devices were divided into two groups (small and large) based on the area of the package surface. Large parts were those larger than the 0.25 inch

diameter XRF spot and small parts were those smaller than the 0.25 inch diameter XRF spot. For this reason, XRF could be used to determine the concentration of bromine in the larger devices but not the smaller devices.

The first step in the analysis was to determine the total bromine and antimony concentration. AAS was used for the antimony concentration as described in the test plan. XRF was used for the bromine concentration in the large devices as described in the test plan. The bromine concentration in the small devices was determined using WDS. WDS was also used to confirm the bromine concentration values in the larger devices. The concentration values are provided in Table 9 below. The second step was to identify the resin types, which were determined by querying the manufacturer. The resin types are also provided for all but two devices in Table 9.

		(%)	%	
		Br conc	**Sb**	**Resin**
Large	DSP	0.420	1.26	Biphenyl
	FPGA	0.400	1.03	Biphenyl
	SRAM	0.749	0.05	OCN
	A/D Converter	0.792	1.62	OCN
	Flash	0.160	0.34	Biphenyl
Small	Op Amp	0.492	1.62	DCPD
	PGA	0.445	2.35	OCN
	Driver	0.800	2.44	
	Trigger	0.099	1.20	

Table 9: Component Flame Retardant Concentration and Resin Type

The results of the measurement of commercial molding compounds showed that the bromine and antimony concentrations are proportional within the biphenyl resin type, and in general, increase or decrease together within a given resin type. This resulted in a

confounding of the results that made it difficult to separate out the bromine from the antimony effect on wirebond lifetime. This will be discussed in more detail later in the paper.

SEM/WDS was used to evaluate the bromine content of the smaller components and to validate the XRF readings for the larger components. The molding compound is composed mainly of filler, which is usually fused silica. To get an accurate percentage by weight of the amount of bromine in the molding compound, the SEM beam diameter must be large (300μm), but the maximum beam width is restricted to 30μm. So, the method adopted was to restrict the beam to 5μm in a non-filler area and measure the bromine percentage in the unfilled resin area and then multiply the result by percentage of resin (vs. filler) in the molding compound to get the total bromine percentage. The filler percentage was obtained by querying the manufacturer and confirmed by area analysis as shown in Table 10 (All pictures are 200μm X 200μm).

Component	Picture	Filler %
FPGA	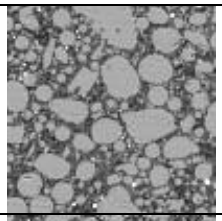	67
A/D Converter	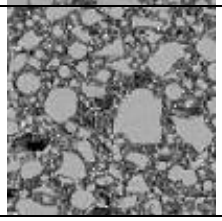	61

		Filler %
Op. Amp.	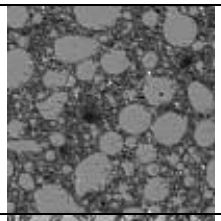	59
Trigger	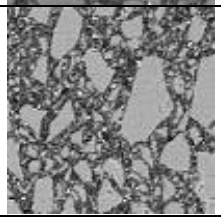	61

Flash Mem	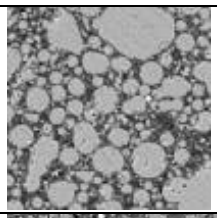	63	PGA	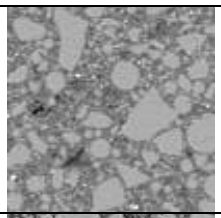	58
SRAM	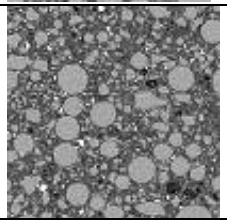	52	Driver	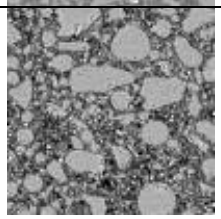	54

Table 10: Filler Percentages by SEM Area Analysis

Experimental Procedure

Once the bromine and antimony concentration in the encapsulant and the type of resin were determined for each device, it was necessary to expose the samples to elevated temperature for extended periods of time and then to determine the intermetallic growth, bond strength degradation, and time-to-electrical failure for each device. This was needed to create a formula for bond strength degradation and/or time-to-failure as a function of bromine and antimony concentration for each resin type.

3) Electrical Testing

A separate experiment was designed to expose a range of plastic encapsulated microcircuits to a high-temperature environment for an extended period of time, and to measure their electrical failure rates based on specific electrical criteria such as read/write

characteristics and voltage levels. The electrical criteria were based on component functionality and different from component to component.

A schematic of the setup is shown along with actual photographs in Table 11.

i) Test Board & Tool-like Chambers	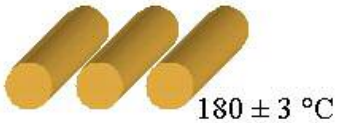	 Test Board  Chambers
ii) Inputs	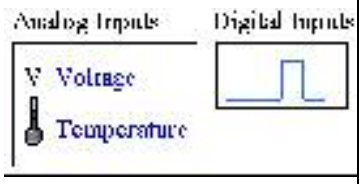	Assembly Front Assembly Rear  
iii) Interface Box		
iv) Data Acquisition	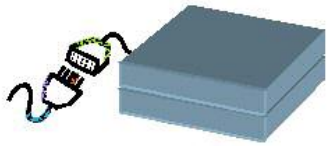	
v) Real-time Monitoring	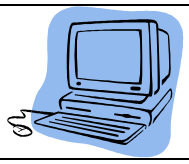	

Table 11: Electrical Test Setup

The devices are assembled on a set of nine boards (referred to as test boards) and the boards are inserted into three tool-like chambers, each holding three test boards. The tool-like chambers are sealed and placed inside the environmental chamber. The wiring from the boards enter the interface box and is routed to the Data Acquisition Unit via the

interface board. The data acquisition unit is connected to the PC via the GPIB interface card.

The main modules involved are :

i. Tool-like chambers with test boards:

These chambers were made exactly like the actual tool enclosure, so that the experiment will closely approximate actual conditions while exposing the components to high temperature. The components were mounted on a test board, which was also close to the actual design. The board also enabled proper electrical routing.

Figure 26: Test Board

ii. Interface box:

The interface box consisted of:

a. Power Supply

b. Interface board

c. Power Protection Board

AC power supply from mains was rectified and controlled with the use of a power protection board, designed to protect the components from electrical surges. The power protection circuit was fabricated on site after electrical design and breadboard testing with a dummy load of large capacitances and high power resistors. It was able to control

the power supply well using relays. After PCB soldering, it was ready for direct use with the system.

iii. Agilent 34970A Data Acquisition Unit:

Each board had one temperature reading, two sets of bit data writing and reading, two sets of voltage input and output and 6 other voltage ouputs. The read/write tests were performed on the memory devices, the voltage input/output tests were performed on the amplifiers. The digital signal processor was monitored separately using a predefined algorithm, and was not connected to the data acquisition unit.

All temperature and voltage signals were handled by routing the wires to 2 40-channel HP34901A multiplexers. The bit data read/write operations were carried out through a serial port and a GPIB card.

iv. PC with GPIB card:

The control of the experiment was handled by a CVI Lab Windows Program, which was used to poll the devices, set time-out limits, handle interrupts, display experiment status, and generate electrical plots.

4) Failure Analysis

Failure analysis was performed on all devices at regular intervals in the experiment. A complete test board was removed at specific intervals and was shipped to the CALCE Electronics Center. The intervals used for failure analysis are as follows:

Board #4 was taken out from oven after 50 Hrs.

Board #6 was taken out from oven after 100 Hrs.

Board #9 was taken out from oven after 150 Hrs.

Board #7 was taken out from oven after 250 Hrs.

Board #2 was taken out from oven after 350 Hrs.

Board #8 was taken out from oven after 515 Hrs.

Board #3 was taken out from oven after 775 Hrs.

Board #5 was taken out from oven after 1300 Hrs.

The following non-destructive experiments were performed as part of the failure analysis:

a) Visual Inspection:

The components were checked for defects such as package cracks, lead corrosion and popcorning.

b) Scanning Acoustic Microscopy:

Scanning Acoustic Micrsocopy (SAM): The SAM uses ultrasound waves to detect the presence of abnormalities such as delaminations in plastic packages. An ultrasonic transducer produces a high frequency sound wave that interacts with the sample. The wave cannot propagate through air, and thus an appropriate medium is used as a couplant. Water is the commonly used couplant. Ultrasound waves freely propagate through liquids and solids, but reflect at boundaries of internal flaws and change of acoustic impedance

(ρC), which is defined as the product of density and longitudinal wave velocity. Acoustic impedances of common package materials are shown in Table 12.

Material	Acoustic Impedance (kg/m^2s)
Water (20°C)	1480000
Air	430
Silicon	20040000
Gold	62530000
Copper	41830000
Aluminum	16900000
Epoxy Resin	3120000

Table 12: Acoustic Impedance of Common Package Materials

A constant frequency signal (usually 15.5 MHz for thick packages) will give rise to signals of varying amplitude and/or phase depending on the reflection coefficient, which is defined as

$$R = [(\rho C)_2 - (\rho C)_1]/[(\rho C)_2 + (\rho C)_1] \qquad 24$$

Thus, a delamination (epoxy-air interface) will show a signal reversal according to equation 24. Comparing the A-Scan image (oscilloscope image) with the Peak Amplitude and Phase Inversion images can give us an accurate idea of the package integrity. This

test was performed on all the packages to determine whether there were any package deformities that could causes stresses around the wirebond area.

c) Decapsulation with fuming HNO_3

The die area was exposed by chemically removing the molding compound. Decapsulation times are usually higher for parts stored at high temperature for longer time, and the decapsulation time varied from 35 seconds to 140 seconds. Etch temperature used in our setup was 85°C. After acidic etching, the component was rinsed with acetone and air-dried for further analyses.

d) Microtesting (Bond Shear)

Bond shear testing was performed on several wires in each sample immediately after decapsulation to find the shear strength of the wirebonds. After cleaning the surface of the die with an air jet, the knife-edge shear tool was placed adjacent to the wirebond and force was applied on the bond by the tool until the resistance was zero (full bond shear). The tool speed was approximately 100 μm/s. If the surface was not properly cleaned, the bond shear machine encountered irregularities and aborted the test. Thus, it was important to decapsulate and clean the die surface properly. Care was also taken not to touch the bonds or reduce their integrity while cleaning. The bond shear force is a measure of the integrity of the bond. Good wirebonds with little porosity require large forces for ductile shear failure through the gold wire ball. Weakened bonds with extensive porosity will fail in a brittle manner at low forces through the corroded intermetallic.

e) Microsectioning

Cross-sectioning was performed to determine the extent of intermetallic growth and subsequent corrosion at the ball-bond to bondpad interface. The samples were re-encapsulated in cold mount compound after bond shear to support the fragile remaining wirebonds and die while sectioning. After mounting, the samples were ground until the required interface was reached. Grinding is done in stages, with decreasing grit size SiC paper. The grades sizes to be used were 240, 400, 600, 800 and 1200. A final polish can also be given using 0.3 μm Al_2O_3 powder, 0.05 μm Al_2O_3 powder, and 0.05 μm colloidal silica.

Results

Electrical data was obtained using the setup described above. The failure range of each device is shown in the following charts (first failure to last failure, in hours).

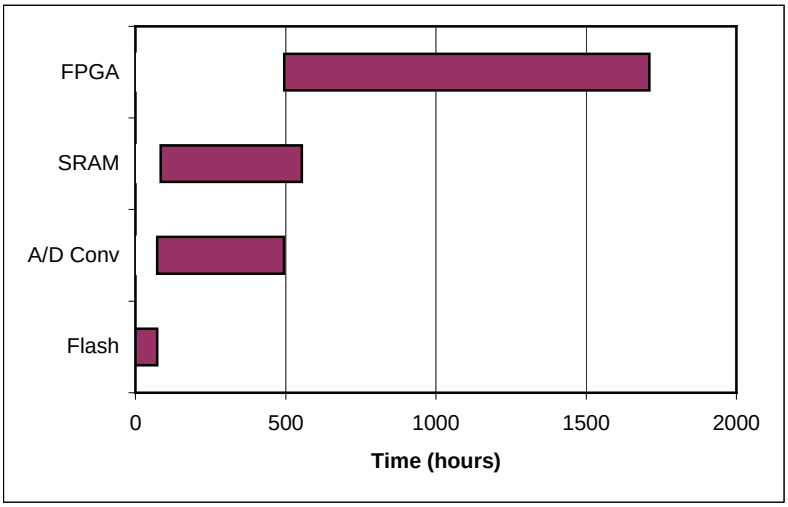

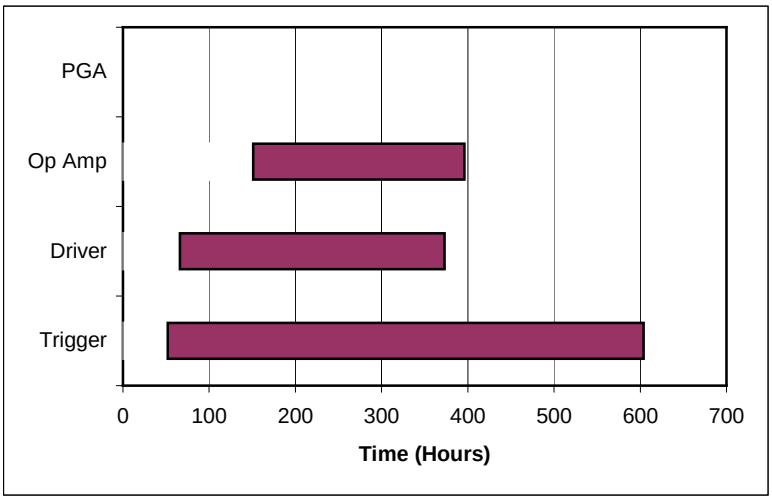

Figure 27: Electrical Failure Range: top) Large Devices bottom) Small Devices

The electrical failure behavior did not correlate well with bond strength degradation or with flame retardant concentration. Reasons for this include the presence of non-uniform, specific, resistance thresholds for electrical failure of each device and the lack of information concerning the thermo-mechanical stress level experienced by each device

during operation. The thermo-mechanical stress is being determined in a follow-on study.

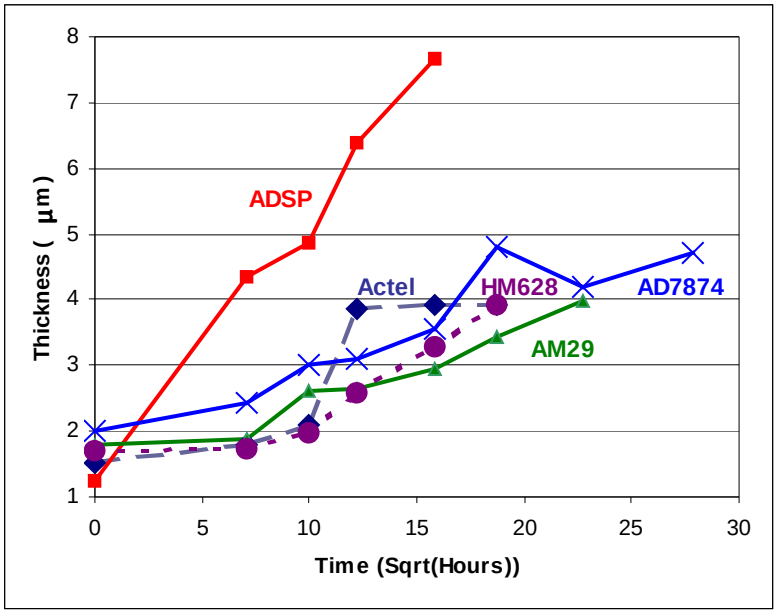

Figure 28: Corrosion/Intermetallic Growth in Large Devices

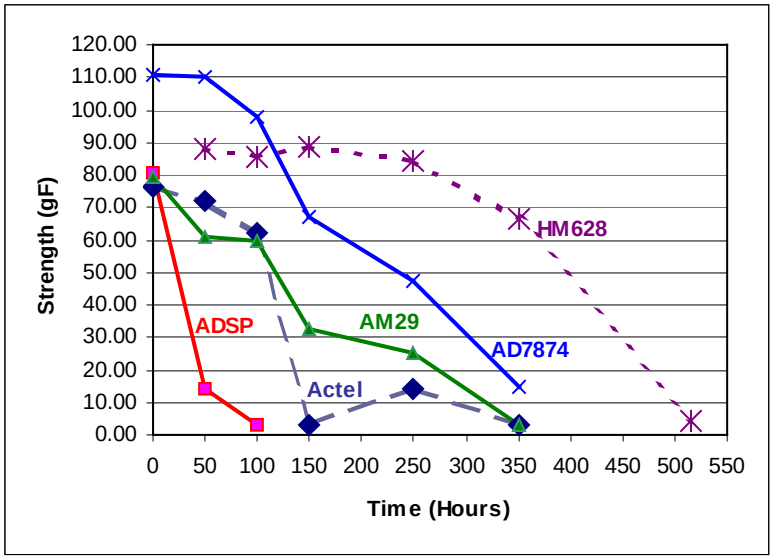

Figure 29: Bond Strength Degradation in Large Devices

Device	Package	Resin	Br (%)	Sb (%)	Tg (°C) Glass Trans.	Tc (°C) Case Temp	Growth Rate	Electrical Failure (Median)	Bond Failure	Corrosion Beyond 4 μm
A/D Converter	SOIC-28	OCN	0.792	1.62	165	184.4	0.183	2	4	3
SRAM	SOP-32	OCN	0.749	0.05		180.0	0.196	3	5	4
DSP	TQFP-100	Biphenyl	0.420	1.26		193.6	0.401	N/A	1	1
FPGA	TQFP-176	Biphenyl	0.400	1.03	145	180.0	0.153	4	2	2
Flash Memory	TSOP-48	Biphenyl	0.160	0.34	135	180.0	0.090	1	3	5

Table 13: Results - Large Devices (Growth rate is in $\mu m/h^{1/2}$)

There is a good correlation between bond failure order, corrosion/intermetallic growth and flame retardant concentration within a resin type. This indicates both a bromine effect and that the type of molding compound resin influences the corrosion of the bond, and subsequent bond strength drop. The bonds encapsulated in Ortho-Cresol Novolac (OCN) resin were found to have a longer life than those encapsulated in Biphenyl resin. The better correlation comes from the fact that bond strength degradation is independent of package stress and electrical failure thresholds, but rather is a direct measurement of the weakening of the wirebond due to corrosion of intermetallics. The poor performance of biphenyl encapsulated packages is troubling, as the trend is to move away from OCN and toward biphenyl as an encapsulant due to its lower moisture absorption and superior resistance to popcorning. However, the trend toward elimination of bromine and antimony from molding compounds to meet the European Union's Restriction of Hazardous Substances (RoHS) legislation should alleviate this concern in newer packages.

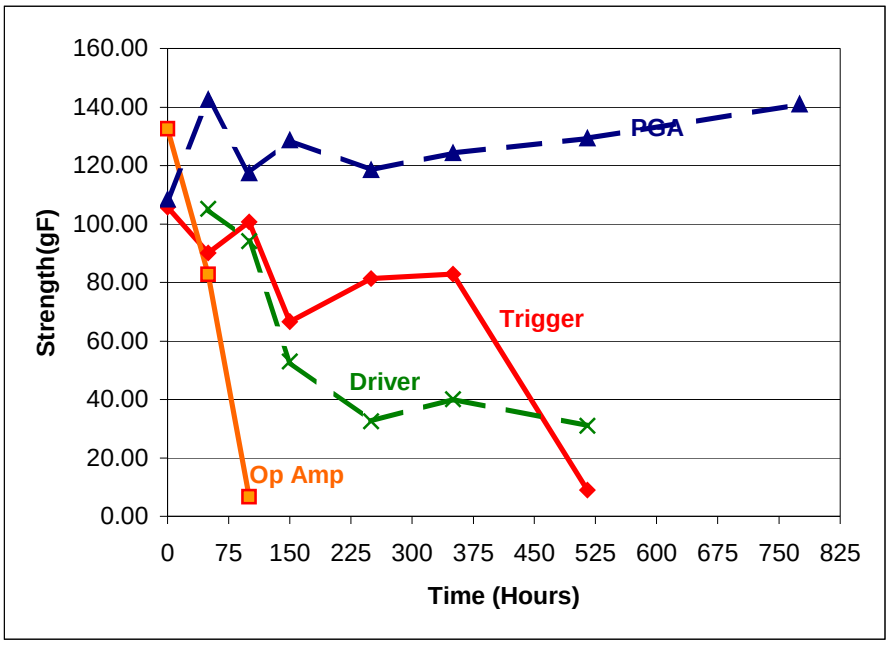

Figure 30: Bond Strength Degradation in Small Devices

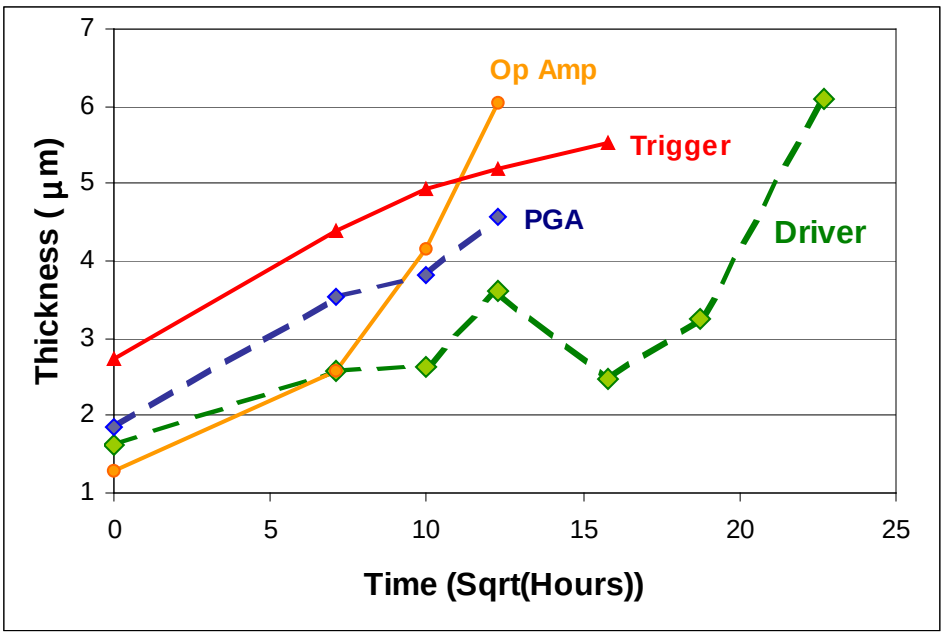

Figure 31: Corrosion/Intermetallic Growth in Small Devices

Device	Package	Resin	Br (%)	Sb (%)	Tg (°C) Glass Trans.	Tc (°C) Case Temp	Growth Rate	Electrical Failure (Median)	Bond Failure	Corrosion Beyond 4 µm
Schimdt Trig	SOIC-14		0.099	1.20		180.0	0.179	3	2	1
Op Amp	SOIC-8	DCPD	0.492	1.62	140-150	180.0	0.661	2	1	2
Prog Gain	SOIC-8	OCN	0.445	2.35	165	180.0	0.214	4	4	3
485 Driver	SOIC-8		0.800	2.44		180.0	0.151	1	3	4
Growth Rate units are µm/√Hour										

Table 14: Results: Small Devices (Growth rate is in $\mu m/h^{1/2}$)

In the smaller devices, similar behavior was observed. Again, OCN-encapsulated bonds survived longer. The encapsulant resin that produced the shortest bond life in this case was dicyclopentadiene (DCPD), however, no devices were found to be encapsulated in biphenyl resins. Since all the resin types could not be obtained from the manufacturers, the resin data set is incomplete in the case of the small devices.

6 Model Development

Early work on an empirical equation to model the degradation of Au-Al bonds has been limited to sample preparations with varying bromine concentrations, and did not focus on the type of resin [17]. Further work in this area by Uno et al. [10] brought the importance of the resin type into the equation, but did not address the concentration of the flame retardant. Thus, there is a need for a complete model to describe the Au-Al interface degradation due to flame retardants in different resin formulations.

Intermetallic growth has been found to have a square-root dependence on time. However, as the degradation of the bond was due to both intermetallic formation and its subsequent corrosion, there was not a one-to-one correspondence between intermetallic thickness and bond shear strength. For this reason, we chose to model bond shear strength degradation directly as the critical dependent parameter. The rate of bond degradation was modeled using an S-curve. This curve brought out the degradation rate much better than a linear model, since each device had varying bond degadation start times or offsets (M), rates (K), initial bond strengths (C), bond strengths at failure (A), and curve exponents (β). An equation (Eq. 25) was developed to model this behavior, and the required exponents were found for each device from the curve in Figure 32.

$$B = C - \frac{C - A}{\left(1 + \beta e^{-K(t-M)}\right)^{\frac{1}{\beta}}} \qquad 25$$

Where

B = bond strength

t = time

M = bond degadation start times or offset

K = rate of degradation

C = initial bond strengths

A = bond strength at failure

β = curve exponents (where the curve slopes more)

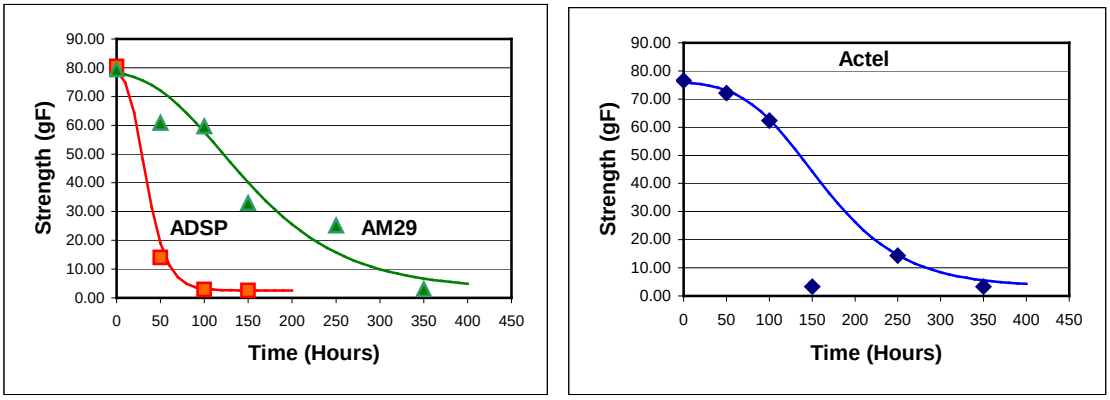

(a) (b)

Figure 32: S-curve Models of Bond Degradation for BP Resin: (a) ADSP & AM29, (b) Actel

From the time dependence of the degradation, one can derive a term "K" that gives the rate of degradation for each molding compound as a function of temperature, type of resin, and concentration of bromine and antimony in the resin. "K" is modeled using a power law for the bromine and antimony concentration and an Arrhenius law dependence

on temperature, where the constants and activation energy vary for different resin types. This model is shown in Eq. 26.

$$K = A[Br]^m[Sb]^n e^{-\frac{E_a}{kT}} \qquad 26$$

Where

K = rate of degradation of the bond

A = pre-exponential factor

m = bromine coefficient

n = antimony coefficient

E_a = activation energy

k = Boltzmann constant

T = temperature (Kelvin)

The choice of actual ICs for testing proved to be a major drawback in determining the constants in this equation. As stated before, bromine and antimony concentrations track each other in actual molding compounds as part of the strategy for flame retardance. As such, the effects of bromine concentration and antimony concentration are confounded and can not be isolated. As this model was intended to predict degradation for high temperature systems where the bromine is the product of thermal decomposition and is affected little by the antimony concentration, we assumed the influence of antimony to be zero. This could also be interpreted as having the antimony influence concealed within the bromine influence.

When the antimony effect was removed, it was possible to determine the activation energy and bromine power law exponent for the biphenyl resin, using the findings of Table 9, specifically those for the ADSP, FPGA and Flash devices. The activation energy, shown in Table 15, confirmed the findings of Uno et al. for biphenyl resin [10], shown in Table 16. Table 15 also provides the power law exponent for the bromine concentration as well.

E_a	m	n	A
1.87 eV	0.29	0.00	5.50E+19

Table 15: Results of Current Study for Biphenyl Molding Compounds

E_a	A
1.8 eV	7.2E+18

Table 16: Results of Uno et al. [10]

Thus, there is an agreement in activation energies and pre-exponential factors between this study and previous studies on Au-Al bonds, but this study has also quantified the flame retardant effect.

Sensitivity Analysis

A sensitivity analysis was performed on the model. Table 17, Table 18 and Table 19 show the sample sets used for bond shear, for the FPGA, the DSP and the Flash, all of which had the biphenyl resin as encapsulant.

FPGA Bond Shear Readings at each time interval

	1	2	3	4	5	6	7	8	9	10
0	64.2	74.7	81.1	71.4	76.2	67.2	74.5	68.9	77.5	81.5
50	67.60	78.30	45.90	92.10	86.40	62.50				
100	58.10	66.80	59.60	66.60	60.50					
150	1.50	2.60	2.30	4.30	2.70	6.40				
250	17.30	12.40	10.80	17.90	17.00	15.50	9.40			
350	5.00	2.00	2.50	4.90	2.70	2.90	3.50	3.10		

515	7.10	5.30	5.40	4.50	4.10
775	5.30	6.90	2.50	5.20	

Table 17: FPGA Bond Shear Readings

DSP Bond Shear Readings at each time interval

	1	2	3	4	5	6	7	8	9	10
0	83.7	72.1	86.5	86.1	74.8	86.4	81.3	91.2	71.5	72.3
50	13.20	14.30	19.20	9.20						
100	5.30	3.00	1.50	2.10	2.30					
150	2.60	2.50								

Table 18: DSP Bond Shear Readings

Flash Bond Shear readings at each time interval

	1	2	3	4	5	6	7	8	9
0	78.1	72.0	73.6	70.4	81.7	80.6	77.5	83.6	96.7
50	59.90	58.70	59.80	60.10	57.40	59.60	70.90	69.20	52.30
100	66.30	60.30	64.60	61.10	58.20	49.80	57.00	57.00	47.80
150	50.10	13.50	43.20	32.10	25.60				
250	25.10								
350	3.20	2.30	3.20	3.10					

Table 19: Flash Memory Bond Shear Readings

The minimum bond shear values for each time interval were used to extract a first bond degradation rate set by fitting Eq. 25. A second bond shear degradation rate set was obtained using Eq. 25, but using the maximum bond shear values. These two sets were used to evaluate constants from Eq. 26 as before, and the new set of values for E_a, A and m were found.

Table 20 shows the range of values generated for E_a, m and K using minimum and maximum bond shear data.

Minimum Bond Shear Data				Mean Bond Shear Data				Maximum Bond Shear Data		
E_a	m	A		E_a	m	A		E_a	m	A
1.84 eV	0.33	4.16E+19		1.87	0.29	5.5E+19		2.07 eV	0.41	1.64E+22

Table 20: Range of values for E_a, m and K

A more uniform number of readouts per point can contribute to a narrower range.

Curve fit for HF compound

The S-curve equation (Eq. 25) was fit to bond shear data of the HF compound at 180 °C. This generated a K (bond degradation rate) of 0.14 /hour. The Flash Memory device which was studied had also used the same type of flame retardant, and the value in that case was 0.13 /hour. It was also aged at 180 °C. The values are approximately equal, as expected. The S-curve for the HF compound is shown in Figure 33.

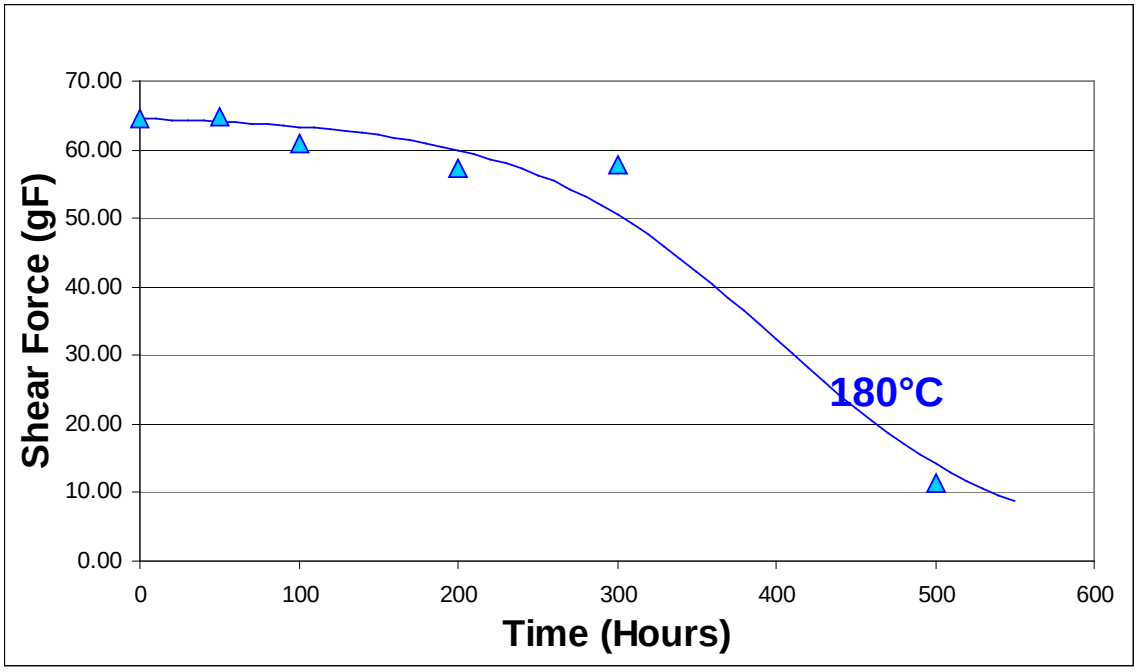

Figure 33: S-curve for HF compound

7 Conclusion

Au-Al bond degradation is an important factor in selecting the most suitable PEM for a high temperature application, and various factors such as flame retardant concentration and T_g of the encapsulant resin have to be considered in this process. Various techniques were used to identify flame retardants in commercial packages. The approach for each technique is not the same as that for a standard sample, since extracting a useful portion of the sample from a commercial package requires a careful experimental procedure, which has been documented.

High temperature storage experiments were conducted on electronic components with different molding compound types. Good correlation was obtained between the bromine concentration, corrosion growth rate and bond strength degradation rate. The results have been used to develop an empirical model of the failures. Failure analysis has been conducted on 9 different part types (5 large and 4 small). The bond strength degradation has been modelled using an S-curve, and a model has been developed to relate it with flame retardant concentration for the biphenyl resin.

To refine the process and the model further, analysis on more types of commercial PEMs is required. For each device, it is possible to extract a single parameter out of the various constants such as m, n, T_g, E_a, M, β, C and so on. This can be done using a transformation matrix, but further data and subsequent validation are required, as mentioned previously.

As a solution to the problem of bromine-related corrosion, two alternate molding compounds : HF and MAR (with lower and no flame retardant chemicals respectively) were tested under high temperature and high humdity. The HF compound gave better wirebond reliability than conventional compounds, as predicted by the model (due to lower bromine concentration), and the MAR gave exceptionaly good wirebond reliability in both high temperature and high humidity.

8 Contributions

1) Independent and complete test of environment-friendly encapsulant under HTSL and HAST conditions for wirebond reliability. Comparison of bond life with conventional encapsulant.
2) Development of a test plan to qualify commercial packages for a high temperature environment by testing the package encapsulant for specific properties and chemical composition.
3) Development of a model to integrate the dependance of wirebond life on flame-retardant concentration and temperature.

9 Appendix A: Failure Analysis: Schlumberger Products

Large Devices

	FPGA	A/D Converter	SRAM
0 hours			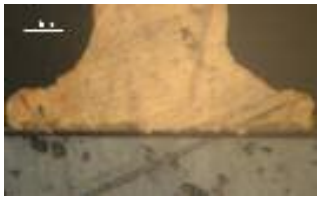
50 hours			
100 hours			
150 hours	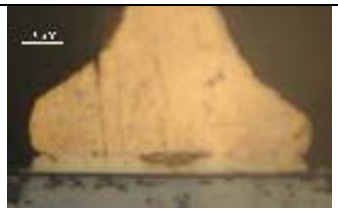		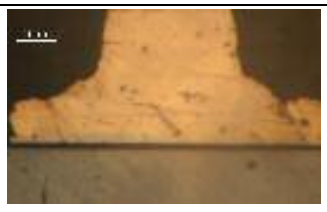

250 hours			
350 hours			
515 hours	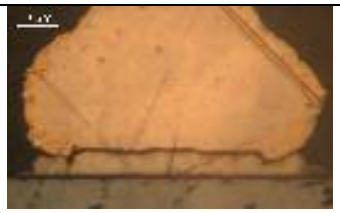		
775 hours			

	Flash	DSP
0 hours		

50 hours	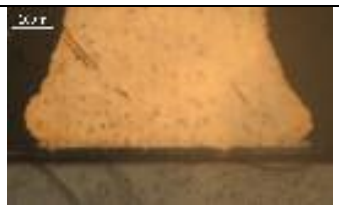	
100 hours		
150 hours		
250 hours	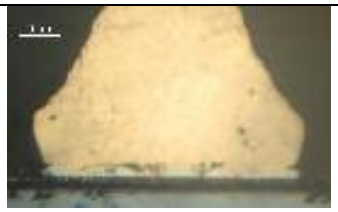	
350 hours		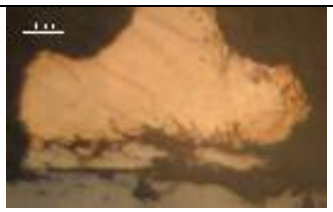
515 hours		
775 hours		

Small Devices

	Schmidt Trigger	PGA
0 hour	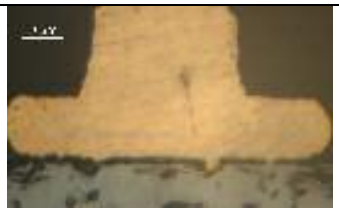	
50 hours	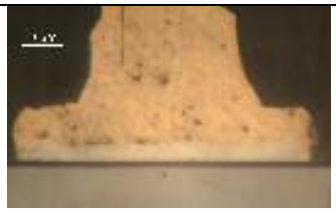	
100 hours		
150 hours	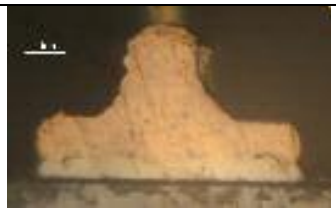	
250 hours	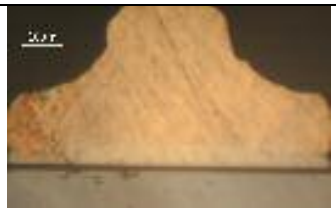	

350 hours	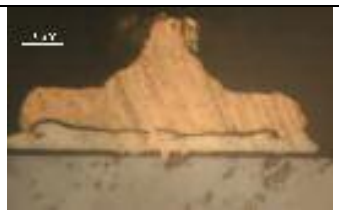	
515 hours		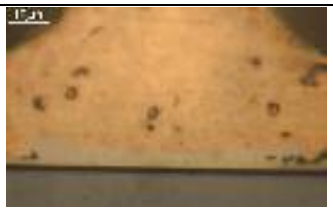
775 hours	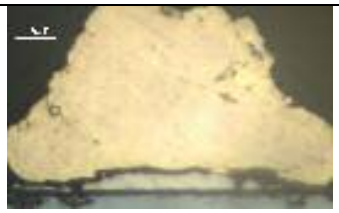	

	Driver	Op Amp
0 hour		
50 hours		

100 hours		
150 hours	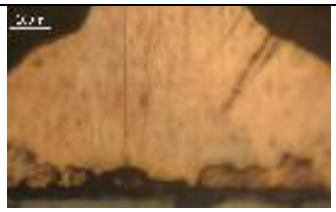	
250 hours		
350 hours	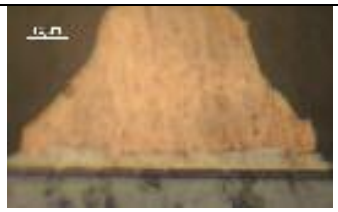	
515 hours	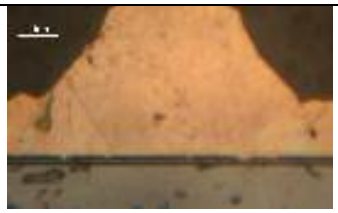	
775 hours		

10 Appendix B: Software Interface Flowchart

This flowchart was used to interface the CVI Lab Windows software with the data acquisition unit during electrical testing.

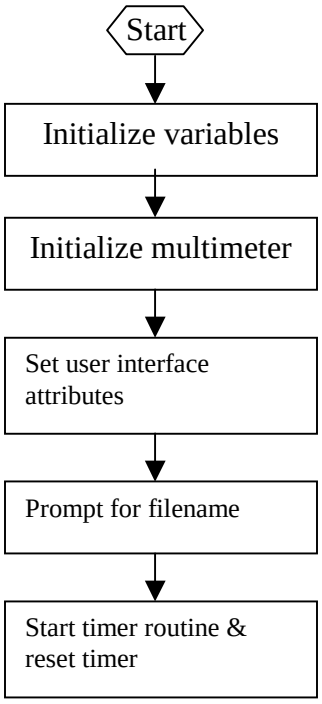

List of CALLBACK functions:

Tic : Timer Interrupt

Display : Displays data for specified board & requested time range

Clear : Clears the display screen

ResetButton : Resets the highest bit

Quit : Quits the program

Sw1 .. Sw10 : Switches for each board

1) Timer Routine : *CVICALLBACK tic*

1.1 Check if user has requested quitting the program, if yes, call **CloseDevices** & exit, if no, go to Step 1.2

1.2 Check for end of array

1.3 Check switch status for each board & get board exit time if required

1.4 Scan temperature

1.5 Initialize current elements of arrays to zero

1.6 Check analog devices

1.7 Read serial port data

1.8 Update main array

1.9 Update temperature array

1.10 Get time instant

1.11 Add data to file

1.12 Display Supply Voltages

1.13 Plot temperature profile

2) Device Status Display : *CVICALLBACK Display*

2.1 Reset text box

2.2 Get Time Range

2.3 Get Board Selection

2.4 Calculate time intervals for 20 display lines

2.5 Display status of devices in text box

3) Clear Display : *CVICALLBACK Clear*

3.1 Clear text box

4) Reset highest bit : *CVICALLBACK ResetButton*

4.1 Confirm Reset

4.2 Reset the highest bit

5) Quit Interface : *CVICALLBACK quit*

5.1 Set ‘running’ variable to OFF

6) Board Switches : *CVICALLBACK Sw1 .. Sw10*

6.1 Confirm

a. If yes, set boardFlag to opposite value

b. If no, reset switch to original value

1.6 Check Analog Devices : AnalogCheck

1.6.1 Assemble channel string based on boards that are ON

1.6.2 Check if Reference voltage is within range

1.6.3 Check if Op-amp output voltage is within range

a. Check positive

b. Check negative

c. Check zero

1.6.4 Check if PGA output voltage is within range for gains 1 & 10

a. Check positive

b. Check negative

c. Check zero

1.6.5 Assemble status word after each check

1.6.6 Set voltages to the Opamp & PGA alternating between +/- (non-measurement duration)

1.7 Read Serial Port Data : ReadSerial

1.7.1 Open Com port

1.7.2 Start ‘for’ loop for boards

1.7.3 Check for preamble & checksum, if matching, go to Step 1.4.11

1.7.4 Reset

1.7.5 Change board to the number in loop

1.7.6 Strobe

1.7.7 Flush serial port

1.7.8 Read data into the buffer

1.7.9 Get preamble

1.7.10 Calculate checksum & preamble, goto Step 1.4.3

1.7.11 Assemble status word

1.7.12 Get status characters of 3 specified devices

1.7.13 Close Com port

1.11 Add Data to File : WriteToFile

1.11.1 Open File

1.11.2 Write string to file

1.11.3 Close File

1.12 Display Supply Voltages

1.12.1 Scan for supply voltages

1.12.2 Display supply voltages (VCC, +5V, -5V) in 3 text boxes

Other Functions :

DAC : It is used in the AnalogCheck function to set the input voltage to a specified value using the multifunction module.

1.3.2 **RefStatus** : Checks if the reference voltage is in a specified range.

1.3.3 **OpAmpStatus** : Checks if the output voltage of the Opamp is within a specified range.

1.3.4 **ChangeGain** : Changes the gain to 1,10 or 100 using the multifunction module digital output.

1.3.5 **PGAStatus** : Checks if the PGA output voltage is within a specified range

1.3.6 **ChangeGain** : Same as 1.3.4

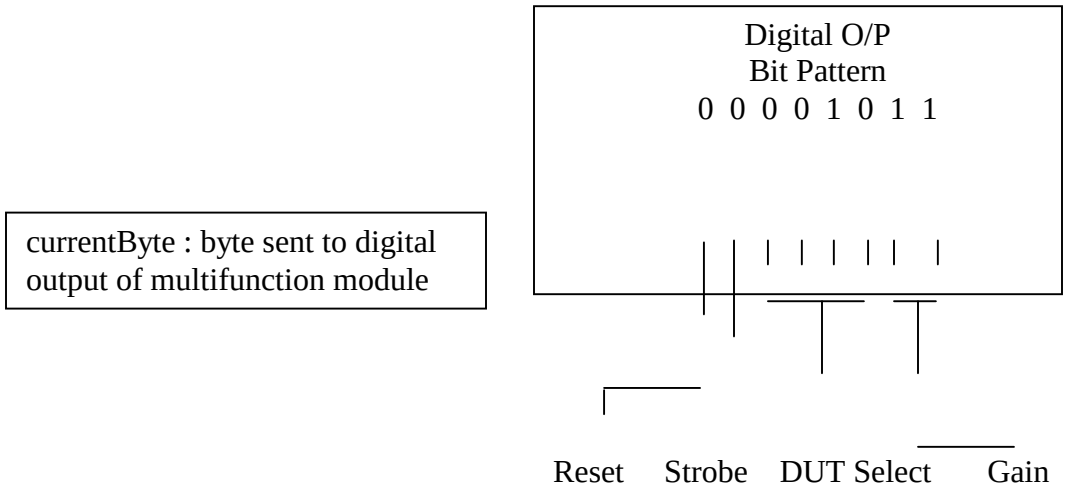

1.4.4 **ResetBoard** : Sets the reset bit to low, high, low and uses 3 writes to the multifunction module's digital output.

1.4.5 **ChangeDUT** : 2 writes to the multifunction module digital output

a. Sets strobe bit to zero.

b. Sets the device to the selected device

1.4.6 **Strobe** : Sets the strobe bit to low, high, low and uses 3 writes to the multifunction module's digital output.

CloseDevices : Stops the Timer & closes the HP34970A & User Interface.

Dec2Bin : Changes input decimal (unsigned short) into a binary format (for display only). The "binary" number is actually a long, but has only 1's and 0's so it is useful while displaying the status of each the boards.

11 Appendix C: Electrical Data for New Molding Compounds

7351:

Number of Failures

	Hours	A	B	C	D	Total	40
180	50	0	0	0	0	0	
	100	0	0	1	1	2	
	200	0	0	1	4	5	
	300	1	0	2	5	8	
	400	3	1	3	5	12	
	500	4	1	3	8	16	
	600	9	4	7	9	29	
	700	10	10	10	10	40	
	800	10	10	10	10	40	
	900	10	10	10	10	40	
	1000	10	10	10	10	40	
	1100	10	10	10	10	40	

Number of Failures

	Hours	A	B	C	D	Total	40
200	50	2	0	1	1	4	
	100	3	0	1	2	6	
	200	10	10	10	10	40	
	300	10	10	10	10	40	
	400	10	10	10	10	40	

Actual Resistance (Ohms)

		A_{mean}	A_{σ}	B_{mean}	B_{σ}	C_{mean}	C_{σ}	D_{mean}	D_{σ}
HAST	0	0.90	0.01	0.82	0.01	0.90	0.02	0.83	0.01
	50	0.90	0.02	0.82	0.02	0.91	0.03	0.84	0.02
	100	0.92	0.03	0.82	0.02	0.91	0.03	0.83	0.02
	200	0.91	0.02	0.83	0.02	0.91	0.02	0.84	0.01
	300	0.91	0.02	0.82	0.02	0.90	0.02	0.84	0.02
	500	0.96	0.04	0.85	0.02	0.93	0.02	0.91	0.05
	600	1.01	0.06	0.89	0.03	0.95	0.02	0.95	0.08
	700	1.05	0.07	0.93	0.04	1.01	0.02	1.02	0.11
	800	1.05	0.06	0.94	0.03	1.02	0.03	1.03	0.13
	900								
	1000								

	A										B									
Sample No. >	6	7	8	9	10	11	12	13	14	15	6	7	8	9	10	11	12	13	14	15
Time																				
50	92	92	89	90	87	86	92	87	92	90	83	84	81	82	79	81	85	81	84	80
100	92	92	89	89	97	97	92	88	91	90	83	85	80	81	81	81	86	82	84	81
200	91	92	91	91	88	89	92	92	93	89	84	85	82	84	83	83	84	82	83	79
300	90	94	92	92	88	90		93	92	90	84	82	81	81	84	83	84	79	82	79
500	94	97	96	97	92	91		104	99	94	86	86	83	85	86	86	86	83	85	82
600	97	100	101	106	96	93		114	101	97	90	87	88	88	90	91	89	95	88	86
700	99	105	102	112	107	98		121	104	100	96	91	93	92	102	97	92	88	92	90

800	99	106	104	110	100	103	120	106	101	95	93	94	92	99	96	97	90	92	94	

	C										D									
Sample No. >	6	7	8	9	10	11	12	13	14	15	6	7	8	9	10	11	12	13	14	15
Time																				
50	96	94	89	90	88	87	92	87	93	90	87	86	82	83	83	80	86	82	84	84
100	96	95	89	90	89	88	92	87	91	90	86	85	82	82	82	80	86	81	84	84
200	93	94	91	93	89	89	93	89	92	89	86	85	82	85	82	84	85	82	84	84
300	91	93	89	91	87	90	91	86	93	90	83	83	82	86	82	88	84	89	83	84
500	96	96	92	91	91	91	97	91	95	93	87	88	85	92	88	99	89	100	87	91
600	97	98	97	93	94	94	98	93	95	95	89	89	90	98	92	104	91	113	90	97
700	101	104	102	99	100	99	103	99	98	101	96	93	100	104	103	108	95	130	93	102
800	102	102	104	100	101	106	105	97	100	105	93	94	95	104	102	108	100	138	96	99

G700:

Number of Failures

	Hours	A	B	C	D	Total	40
180	50	0	0	0	0	0	
	100	0	0	1	1	2	
	200	0	0	1	4	5	
	300	1	0	2	5	8	
	400	3	1	3	5	12	
	500	4	1	3	8	16	
	600	9	4	7	9	29	
	700	10	10	10	10	40	
	800	10	10	10	10	40	
	900	10	10	10	10	40	
	1000	10	10	10	10	40	
	1100	10	10	10	10	40	

Number of Failures

	Hours	A	B	C	D	Total	40
200	50	2	0	1	1	4	
	100	3	0	1	2	6	
	200	10	10	10	10	40	
	300	10	10	10	10	40	
	400	10	10	10	10	40	

Actual Resistance (Ohms)

		A_{mean}	A_{σ}	B_{mean}	B_{σ}	C_{mean}	C_{σ}	D_{mean}	D_{σ}
HAST	0	0.87	0.01	0.80	0.01	0.88	0.01	0.79	0.01
	50	0.87	0.02	0.80	0.01	0.88	0.02	0.79	0.02
	100	0.87	0.03	0.80	0.01	0.88	0.02	0.80	0.01
	200	0.87	0.02	0.80	0.02	0.88	0.02	0.80	0.01
	300	0.86	0.03	0.79	0.03	0.87	0.03	0.80	0.02
	500	0.87	0.02	0.81	0.02	0.89	0.03	0.81	0.02
	600	0.88	0.03	0.82	0.02	0.90	0.02	0.82	0.02
	700	0.89	0.03	0.82	0.02	0.91	0.02	0.84	0.05

Sample No. >	A										B									
Time	6	7	8	9	10	11	12	13	14	15	6	7	8	9	10	11	12	13	14	15
0																				
50	85	88	84	87	83	90	90	85	86	88	77	82	78	80	79	81	80	79	79	80
100	83	88	83	87	85	91	89	86	87	88	79	82	79	81	81	81	82	79	81	79
200	85	87	84	87	85	91	89	84	87	90	79	83	77	82	76	80	81	81	81	79
300	86	90	84	87	87	91	88	82	83	86	80	85	78	84	77	79	79	76	77	78
500	85	87	84	88	85	91	90	85	87	89	78	83	80	80	79	81	85	79	81	81
600	85	91	84	89	86	93	91	86	87	91	81	85	80	83	79	83	82	80	83	83
700	86	92	85	89	85	93	91	86	89	90	80	85	83	84	80	83	84	80	82	81

Sample No. >	C										D									
Time	6	7	8	9	10	11	12	13	14	15	6	7	8	9	10	11	12	13	14	15
0																				
50	86	91	86	88	87	90	90	86	89	88	79	82	78	78	78	82	83	77	79	78
100	84	91	85	87	86	90	89	87	89	89	78	81	78	79	80	82	81	78	81	79
200	87	90	86	87	87	90	90	87	89	89	81	80	79	80	79	82	82	79	82	80
300	88	93	86	88	84	88	88	84	87	87	82	83	79	80	78	82	80	76	77	82
500	86	91	85	88	88	90	91	86	92	91	81	81	80	80	81	84	84	79	80	84
600	87	93	87	90	88	92	93	87	91	91	81	83	80	80	80	86	85	80	81	84
700	89	93	89	94	89	93	93	87	93	91	84	84	82	81	81	86	85	83	81	97

REFERENCES

[1] McCluskey F.P, Grzybowski R., and Podlesak T., "High Temperature Electronics", *CRC Press, Inc., New York, NY, 1997*

[2] Bennett G, "Thermal Protection Methods For Electronics in Hot Wells", *High Temperature Microelectronics, Kirschman R, Ed., IEEE Press, Piscataway, NJ (1998) pp.111-124*

[3] Harman, G. "Metallurgical bonding systems for high-temperature electronics," *High-Temperature Microelectronics, Kirschman, R., ed., IEEE Press, Piscataway, NJ pp. 752-769*, 1998.

[4] G.E.Servais, S.D.Brandenburg, "Wire Bonding – A Closer Look", Delco Electronics Corp., Kokomo, IN., *ISTFA'91: The 17th International Symposium for Testing & Failure Analysis, Los Angeles, California, USA (1991)*

[5] Philofsky. E., "Intermetallic Formation In Gold-Aluminum Systems", Motorla Inc., Semiconductor Products Division, *Solid-State Electronics, Permagon Press Vol 13., pp. 1391-1399 (1970)*

[6] International Agency for Research on Cancer (IARC) - Summaries & Evaluations *vol 47, p.291 (1989)*

[7] Material Safety Data Sheet: Bromine, Mallinckrodt Chemicals, NJ, USA. *(2001)*

[8] Ampacet Corporation – "Flame Retardants" *(http://www.ampacet.com)*

[9] The European Flame Retardants Association – "How Flame Retardants Work" *(http://www.cefic-efra.org)*

[10] Uno T., Tatsumi K., "Thermal Reliability of gold-aluminum bonds encapsulated in bi-phenyl epoxy resin", *Microelectronics Reliability v.40, p145-153 (2000)*

[11] R.E.Thomas, V.Winchell, K.James, T.Scharr, "Plastic Outgassing-Induced Wire Bond Failure", *Proceedings of the 27th Electronics Components Conference, 1977, pp. 182-187, 1977.*

[12] Khan M., Fatemi H., Romero J., Delenia E., "Effect of high thermal stability mold material on the gold-aluminum bond reliability in epoxy encapsulated VLSI devices." *26th Annual Proceedings. Reliability Physics New York, NY, USA: IEEE, p. 40-9(1988)*

[13] W.M. Paulson, R.P. Lorigan, "The Effect of Impurities on the Corrosion of Aluminum Metallization", *Proceedings of the IEEE International Reliability Physics Symposium, 1987.*

[14] Khan M., Fatemi H., "Gold-Aluminum Bond Failure Induced By Halogenated Additives in Epoxy Molding Compounds", *Proceedings of the 1986 International Symposium on Microelectronics. Reston, VA, USA: Int. Soc. Hybrid Microelectron, p. 420-8 (1986)*

[15] R.J. Gale, "Epoxy Degradation Induced Au-Al Intermetallic Formation in Plastic Encapsulated MOS Memories", *Proceedings of the IEEE International Reliability Physics Symposium, 1984.*

[16] Imasato E., Araki M., Shimizu I., Ohno Y., "Effect of Mold Resin of Reliability in Gold-Aluminum Bonding", *Proceedings of 2nd Electronics Packaging Technology Piscataway, NJ, USA, IEEE p. 338-44 (1998)*

[17] Ahmad S., Blish R., Corbett T., King J., "Effect of bromine concentration in molding compounds on gold ball bonds to aluminum bonding pads." *36th*

Electronic Components Conference Proceedings. New York, NY, USA: IEEE p. 127-31 (1986)

[18] Gallo A.,"Effect of Mold Compounds on Moisture-Induced Degradation of Gold-Aluminum Bonds in Epoxy Encapsulated Devices", *28th Annual Proceedings. Reliability Physics 1990 (Cat. No.90CH2787-0). New York, NY, USA: IEEE,. p. 244-51(1990)*

[19] Gallo A., Dexter Electronic Materials, "Green Molding Compounds" *Technology Information Technical Paper, (2000)*

[20] X-Ray Flouresence Spectroscopy, *Amptek, (http://www.amptek.com/xrf.html)*

[21] Kenneth Priers, "An Introduction to Ion Chromatography", *General Chemistry Laboratory, Calvin College*

[22] Extreme temperature electronics: Technology for the 21st Century, Webbook, CALCE Electronics Center.

[23] Nguyen, L.T., "Reliability of Postmolded IC Packages", *Transactions of the ASME. Journal of Electronic Packaging, vol.115, no.4, p. 346-55 (1993)*

[24] L.G. Feinstein, "Do Flame Retardants Affect the Reliability of Molded Plastic Packages ?", *30th Electronic Components Conference Proceedings, 1980*.